EUROPEAN RESPIRATORY *journal*

FLAGSHIP SCIENTIFIC JOURNAL OF ERS

Early View

Original article

Crucial role of fatty acid oxidation in asthmatic bronchial smooth muscle remodelling

Pauline Esteves, Landry Blanc, Alexis Celle, Isabelle Dupin, Elise Maurat, Nivea Amoedo, Guillaume Cardouat, Olga Ousova, Lara Gales, Florian Bellvert, Hugues Begueret, Matthieu Thumerel, Jean-William Dupuy, Nicolas Desbenoit, Roger Marthan, Pierre-Olivier Girodet, Rodrigue Rossignol, Patrick Berger, Thomas Trian

Please cite this article as: Esteves P, Blanc L, Celle A, *et al*. Crucial role of fatty acid oxidation in asthmatic bronchial smooth muscle remodelling. *Eur Respir J* 2021; in press (https://doi.org/10.1183/13993003.04252-2020).

Crucial role of fatty acid oxidation in asthmatic bronchial smooth muscle remodelling

Pauline Esteves[1,2], Landry Blanc[1,4], Alexis Celle[1,2], Isabelle Dupin[1,2], Elise Maurat[1,2], Nivea Amoedo[1,2], Guillaume Cardouat[1,2], Olga Ousova[1,2], Lara Gales[5], Florian Bellvert[5], Hugues Begueret[3], Matthieu Thumerel[1,2,3], Jean-William Dupuy[1,4], Nicolas Desbenoit[1,4], Roger Marthan[1,2,3], Pierre-Olivier Girodet[1,2,3], Rodrigue Rossignol[1,2], Patrick Berger[1,2,3*] and Thomas Trian[1,2*]

AFFILIATIONS

[1] Univ-Bordeaux, Centre de Recherche Cardio-thoracique de Bordeaux, U1045, MRGM, Functional Genomics Center (CGFB), CIC 1401, CELLOMET, F-33000 Bordeaux, France.

[2] INSERM, Centre de Recherche Cardio-thoracique de Bordeaux, U1045, U1211, CIC 1401, F-33000 Bordeaux, France.

[3] CHU de Bordeaux, Service d'exploration fonctionnelle respiratoire, Service de chirurgie thoracique, Service d'anatomopathologie, CIC 1401, Bordeaux, France

[4] CNRS, UMR5248, Institute of Chemistry & Biology of Membranes & Nano objects, Functional Genomics Center (CGFB), Proteomics Facility, Université de Bordeaux, 33000 Bordeaux, France

[5] Université de Toulouse, CNRS 5504, INRA 792, INSA Toulouse, Toulouse Biotechnology Institute, Bio & Chemical Engineering, MetaToul, Toulouse, France

* Co-last author

CORRESPONDING AUTHOR: Thomas TRIAN, PhD

Centre de recherche Cardio-thoracique de Bordeaux INSERM U1045

PTIB - Hôpital Xavier Arnozan, Avenue du Haut Lévêque, 33600 PESSAC

Tel: (+33) 5 47 30 27 50 e-mail: thomas.trian@u-bordeaux.fr

CONFLICT OF INTEREST DISCLOSURE STATEMENT:

- P. Berger reports grants and personal fees from Novartis; grants, personal fees and non-financial support from Boehringer Ingelheim; personal fees and non-financial support from Chiesi, AstraZeneca, and Sanofi; personal fees from Menarinni, and TEVA, outside the submitted work; In addition, he has a delivered patent (EP N°15152886.6 *i.e*., New compositions and methods of treating and/or preventing Chronic Obstructive Pulmonary Disease), a submitted patent (22605-FR, *i.e*., Geometric characterization of airways using MRI) and a submitted patent (EP N°20173595.8 *i.e*., New compositions and methods of treating COVID-19 Disease), all outside the submitted work.

- PO. Girodet reports research support from AstraZeneca outside the submitted work. In addition, he has a delivered patent (EP 15152886.6 *i.e*., New compositions and methods of treating and/or preventing Chronic Obstructive Pulmonary Disease) and a submitted patent (EP N°20173595.8 *i.e*., New compositions and methods of treating COVID-19 Disease), all outside the submitted work.

- I. Dupin has a delivered patent (EP 15152886 *i.e*., New compositions and methods of treating and/or preventing Chronic Obstructive Pulmonary Disease), and a submitted patent (EP N°20173595.8 *i.e*., New compositions and methods of treating COVID-19 Disease), all outside the submitted work.

- All other authors have no conflict of interest

SOURCES OF FUNDING : The “Fondation de l’Université de Bordeaux” for the FGLMR/AVAD funding, the “Fondation pour la Recherche Médicale” (DEQ20170336706) and “the Agence Nationale pour la Recherche” (ANR, ROSAE project CE14-0015-01). LB acknowledges the “Fondation pour la Recherche Médicale” (ARF201809007123) for personal salary. The COBRA cohort is promoted by INSERM and funded by AstraZeneca, GlaxoSmithKline, Chiesi, Novartis and Roche.

ABSTRACT

Background: Bronchial smooth muscle (BSM) remodelling in asthma is related to an increased mitochondrial biogenesis and enhanced BSM cell proliferation in asthma. Since (i) mitochondria produce the highest levels of cellular energy and (ii) fatty acid beta-oxidation is the most powerful way to produce ATP, we hypothesized that, in asthmatic BSM cells, energetic metabolism is shifted towards the beta-oxidation of fatty acids.

Objectives: We aimed to characterize BSM cell metabolism in asthma both *in vitro* and *ex vivo* to identify a novel target for reducing BSM cell proliferation.

Methods: Twenty-one asthmatic and 31 non-asthmatic patients were enrolled. We used metabolomic and proteomic approaches to study BSM cells. Oxidative stress, ATP synthesis, fatty acid endocytosis, metabolite production, metabolic capabilities, mitochondrial networks, cell proliferation and apoptosis were assessed on BSM cells. Fatty acid content was assessed *in vivo* using MALDI-spectrometry imaging.

Results: Asthmatic BSM cells were characterized by an increased rate of mitochondrial respiration with a stimulated ATP production and mitochondrial β-oxidation. Fatty acid consumption was increased in asthmatic BSM both *in vitro* and *ex vivo*. Proteome remodelling of asthmatic BSM occurred via 2 canonical mitochondrial pathways. The levels of CPT2 and LDL-receptor, which internalize fatty acids through mitochondrial and cell membranes, respectively, were both increased in asthmatic BSM cells. Blocking CPT2 or LDL-receptor drastically and specifically reduced asthmatic BSM cell proliferation.

Conclusion: This study demonstrates a metabolic switch towards mitochondrial beta-oxidation in asthmatic BSM and identifies fatty acid metabolism as a new key target to reduce BSM remodelling in asthma.

Words count: 249

KEY-WORDS: asthma, cell proliferation, mitochondria, LDL-R, metabolism.

INTRODUCTION

Asthma is the most common chronic airway disease and causes a substantial health and economic burden worldwide. According to the Global Initiative for Asthma (GINA), asthma is a heterogeneous disease defined by a history of respiratory symptoms, which vary over time and in intensity, together with variable expiratory airflow limitations [1].

Asthma pathophysiology involves chronic inflammation of both large and small airways, as well as bronchial remodelling [2]. The most crucial feature of bronchial remodelling appears to be BSM increased mass, associated with a reduced lung function [3, 4] and an increased exacerbation rate [5] which are poor prognostic indicators in asthma. Moreover, BSM remodelling can begin very early in life, often at preschool age, and predicts the persistence of asthma in school-age children [6]. Thus, BSM remodelling plays a crucial role in asthma pathophysiology, and there is an unmet need to pharmacologically target BSM remodelling [7].

BSM hyperplasia appears to be the primary feature of BSM remodelling related to an increase in cell proliferation in asthmatic BSM both *in vitro* [8-10] and *ex vivo* [4] compared to non-asthmatic subjects. We previously demonstrated that this increased proliferation of BSM cells from severe asthmatic patients was associated with increased mitochondrial biogenesis and mass [8]. However, although gallopamil, a calcium channel blocker, normalized mitochondrial biogenesis and cell proliferation *in vitro* [8], it only minimally reduced BSM mass *in vivo* [11], suggesting that other pathways are involved in this phenomenon. We also observed that BSM remodelling was associated with an increased mitochondrial mass in nonsevere asthmatic patients, as patients with a high BSM mass presented a higher mitochondrial mass within their BSM [5]. Finally, we previously demonstrated that the increased BSM cell proliferation was more related to mitochondrial respiration than to anaerobic glycolysis in severe asthma [8].

Among the variety of sources of mitochondrial respiration, fatty acid beta-oxidation is the most powerful way to produce ATP in various cell types [12]. For instance, a link between fatty acid metabolism and cell proliferation has been previously demonstrated in hepatocytes [13] and cancer cells [14]. Moreover, the blood concentration of LDL, a source of fatty acids in various cell types after interaction with its receptor [15-17] is negatively correlated with FEV1 in asthma [25].

Therefore, we hypothesized that BSM metabolism was shifted, in asthmatic BSM cells, towards the beta-oxidation of fatty acids, which may represent a potential target to reduce BSM cell proliferation in asthmatic patients.

METHODS

A complete description of all methods used in this study is supplied as supplemental data.

Study population

Patients with asthma and non-asthmatic subjects were prospectively recruited from the "Centre Hospitalier Universitaire (CHU)" of Bordeaux, France, according to the Global Initiative for Asthma [1]. Asthmatic patients were recruited from the "COBRA" cohort (COhort of BRonchial obstruction and Asthma, ethics committee number: 2008-A00294-51/1). Non-asthmatic subjects were recruited after surgical resection. This study received approval from the local and national ethics committees. Bronchial specimens from all subjects were obtained by either fiberoptic bronchoscopy or lobectomy in macroscopically normal areas, as previously described [18].

Cell culture

BSM cells were obtained from patient biopsies and bronchi dissected out from lobectomy, as previously described [8]. BSM cells were then used to assess cell proliferation (by manual counting, BrdU and flow cytometry), cell apoptosis (by luminescent assay), oxidative stress (using OxyBlot), oxygen consumption rate (using Oroboros), cellular and mitochondrial ATP synthesis (by bioluminescence), and various protein contents (by western blot). The mitochondrial network was visualized by immunostaining (TOMM20).

BSM cell metabolites were quantified using 25 mM of [U-^{13}C]glucose and mass spectrometry. Fatty acid endocytosis was assessed by means of fluorescent BODIPY-ceramide. The metabolic capabilities of BSM cells were characterized via redox reactions associated with cellular

respiration. CPT1 and/or CPT2 were inhibited using either pharmacologic (using etomoxir or perhexilin) or genetic silencing (using dedicated lentivirus) methods. The LDL receptor was inhibited by using a blocking antibody.

Proteomic analysis

Cells and tissue lysates were processed using RIPA buffer. Each lysate was centrifuged and supernatants were used for the proteomic analysis at the Mass Spectrometry facility of Bordeaux University, as recently described [19]. Briefly, proteomic analysis was performed using an Ultimate 3000 RSLC Nano-UPHLC system (Thermo Fisher Scientific, Waltham, MA) coupled to a nanospray Orbitrap Fusion™ Lumos™ Tribrid™ Mass Spectrometer (Thermo Fisher Scientific, Waltham, MA).

Matrix-Assisted Laser Desorption/Ionization (MALDI) - mass spectrometry imaging analysis

Patient biopsies were frozen at -80°C and subsequently embedded in a gel of 5% carboxymethyl cellulose. Serial cryo-sections (12 µm-thick) were cut from bronchial biopsies at -20°C using a NX70 Star cryostat (Thermo Fisher Scientific) and thaw-mounted onto standard glass microscope slides for MALDI - mass spectrometry imaging. These acquisitions were performed using a high performance atmospheric pressure imaging ion source called AP-SMALDI 5 AF (TransMIT GmbH) connected to an orbital trapping mass spectrometer (QExactive Orbitrap, Thermo Fisher Scientific). After MALDI - mass spectrometry imaging, we performed an α-smooth muscle actin immunostaining to localize the BSM area. We then estimated the relative

lipid content within the BSM on the MALDI images. Fatty acid annotation was performed using the Human Metabolome Data Base and METASPACE software.

RESULTS

Patients' characteristics

We recruited 21 asthmatic patients and 31 non-asthmatic subjects, whose characteristics are presented in Table 1. Unsurprisingly asthmatic patients exhibited reduced forced expiratory volume in one sec (FEV1) compared to that observed in the non-asthmatic subjects.

Cell proliferation and mitochondrial mass are increased in asthmatic BSM

We initially confirmed that asthmatic BSM cell proliferation was increased compared to that of non-asthmatic subjects through manual cell counting, BrdU and flow cytometry assays (Figure 1A-C). As previously demonstrated [8], no change in apoptosis was observed between the two groups (Figure 1D). Furthermore, cellular oxidative damage, such as protein carbonylation was not different between non-asthmatic and asthmatic BSM cells, indicating oxidative stress was not implicated in the proliferative processes (Figure 1E). Quantification of TOMM20 immunostaining exhibited an increase in the mitochondrial network in asthmatic BSM cells (Figure 1F). We also demonstrated that mitochondrial mass was significantly increased in asthmatic BSM cells using three complementary markers (*i.e.*, porin, citrate synthase and TOMM20, Figure 1G-I).

Mitochondrial bioenergetic function is enhanced in asthmatic BSM

Functional evaluation of the mitochondrial bioenergetics of BSM cells revealed an increased rate of mitochondrial respiration along with a higher maximal capacity in asthmatic BSM cells compared to that observed in the non-asthmatic subjects (Figure 2A). The steady-state ATP content was significantly increased in asthmatic BSM cells compared to BSM cells from non-

asthmatic subjects (Figure 2B). Interestingly, half of this ATP production was sensitive to the inhibition of oxidative phosphorylation (OXPHOS) by rotenone, antimycin and potassium cyanide (Figure 2C).

Glucose oxidative catabolism is stimulated in asthmatic BSM cells

As glucose metabolism is a major pathway in cellular bioenergetics, we investigated the fate of glucose using tracing methods. Levels of ^{13}C-pyruvate (Figure 2D), ^{13}C-succinate (Figure 2E) and ^{13}C-malate (Figure 2F) were significantly increased in asthmatic BSM cells compared to those of non-asthmatic subjects. However, no difference in glucose uptake was observed between the asthmatic and non-asthmatic BSM cells (Figure 2G), whereas lactate production was decreased in asthmatic BSM cells (Figure 2H), suggesting a stimulation of oxidative catabolism. Accordingly, a significant increase in ^{13}C-ATP was also observed in asthmatic BSM cells (Figure 2I). These results strongly confirmed the increase in tricarboxylic acid (TCA) cycle activity in asthmatic BSM cells. Since the TCA cycle can be fuelled by numerous anaplerotic sources in addition to glucose, we performed an unbiased proteomics investigation to identify additional changes in cell metabolism.

Proteome remodelling reveals a stimulation of the fatty-acid oxidation system in asthmatic BSM

Raw data from the label-free proteomics approach were shared through PRIDE (under accession number PXD015566) and revealed significant modifications in the expression of 213 proteins ($p<0.05$). Using Ingenuity Pathway Analysis, we demonstrated significant alterations in various canonical pathways including ‘mitochondrial dysfunction’ and ‘oxidative phosphorylation’

(Figure 3A), in complete agreement with the above-described stimulation of mitochondrial bioenergetics in asthmatic BSM cells. Moreover, after analysing the specific up- and downregulated proteins in asthmatic BSM cells, we focused our attention on carnitine palmitoyl transferase-2 (CPT2), since it was the most significantly upregulated protein [3.063-fold increase ($p=0.016$)] among the "mitochondrial dysfunction" annotation box in asthmatic BSM cells compared to that observed in the non-asthmatic BSM cells (Figure 3B and Supplemental table 1). CPT2 is a mitochondrial fatty acid transporter allowing that allows fatty acids to follow the β-oxidation pathway for ATP production. CPT2 expression was significantly increased in asthmatic BSM cells *in vitro* compared to that in BSM cells from non-asthmatic subjects (Figure 3C).

Fatty acid consumption is specifically strengthened in asthmatic BSM

To be metabolized, fatty acid molecules first need to enter BSM cells through LDL-R, one of the primary cell surface receptors for triglyceride-enriched lipoproteins. We observed a significant increase in LDL-R protein expression *in vitro* in asthmatic BSM compared to that observed in the non-asthmatic subjects (Figure 4A). We next assessed the short term (*i.e.*, 20 min) fatty acid endocytosis by asthmatic and non-asthmatic BSM cells using BODIPY lipid ceramide, a fluorescent tool for the analysis of fatty acid endocytosis (Figure 4B). We observed significantly increased fluorescence within asthmatic BSM cells, indicating increased absorption into asthmatic BSM cells (Figure 4C). BODIPY fluorescent lipid ceramide uptake by BSM cells was also quantified using a fluorimeter, with the results showing a significant increase in absorption by asthmatic BSM cells compared to BSM cells from non-asthmatic subjects (Figure 4D). Moreover, to confirm that fatty acid consumption by asthmatic BSM cells was increased in

asthmatic BSM cells, we measured the resting concentrations of fatty acids in the culture medium of asthmatic and non-asthmatic BSM cells. As expected, we observed a significantly lower resting concentration of fatty acids in asthmatic BSM cell medium compared to that the in non-asthmatic cell medium (Figure 4E). To elucidate the capacity of BSM cells to perform OXPHOS associated with fatty acid oxidation, we used a Biolog Mitoplate assay, which measures the reduction of cytochrome c [20], an intermediate of the respiratory chain. Using palmitoyl-DL-carnitine as a unique energetic substrate for BSM cells, we observed a significant increase in the dye reduction by asthmatic BSM cells, suggesting a higher level of OXPHOS associated with fatty acid oxidation (Figure 4F).

To further assess fatty acid metabolism *in vivo*, we performed MALDI - mass spectrometry imaging of asthmatic and non-asthmatic bronchial biopsy slices. Using BSM immunostaining following mass spectrometry imaging, we estimated the relative lipid content within BSM (Figure 5 and Supplemental figure S1). Among the most representative fatty acids, we observed a significant decrease in arachidonic (Figure 5A), stearic (Figure 5B), and linoleic (Figure 5C) acid contents in asthmatic BSM compared to those observed in the non-asthmatic subjects. However, the difference in the palmitic acid content between asthmatic and non-asthmatic BSM did not reach statistical significance ($p=0.06$) (Figure 5D). To assess the BSM tissue specificity of this increased consumption of fatty acids, we performed the same analysis for the bronchial epithelium of the same biopsies. There were no alterations in the contents of any of the tested fatty acids between asthmatic and non-asthmatic bronchial epithelial layers (Figure 5E-H).

Taken together, these results demonstrated that the fatty acid consumption-mediated increase in mitochondrial metabolism was specifically increased in asthmatic BSM both *in vitro* and *ex vivo*.

Inhibition of fatty acid oxidation specifically impedes asthmatic BSM cell proliferation

We next assessed whether the specific increase in fatty acid metabolism within asthmatic BSM was required for BSM cell proliferation. To shut down the fatty acid oxidation pathway, we first inhibited CPT1 and CPT2 activities using etomoxir (Figure 6A and 6B) and perhexilin (Figure 6C and 6D), which both significantly decreased the proliferation of asthmatic BSM cells. However, neither compound affected non-asthmatic BSM cell proliferation. Moreover, the proliferation of bronchial epithelial cells was not affected by either etomoxir or perhexilin (Supplemental figure S2A and S2B), again suggesting a specific role of mitochondrial fatty acid metabolism in asthmatic BSM cell proliferation. Subsequently, we demonstrated that both etomoxir and perhexilin significantly decreased basal respiration in asthmatic, but not non-asthmatic BSM cells (Figure 6E). To further confirm the crucial role of CPT2 in asthmatic BSM cell proliferation, we used a silencing strategy with a lentivirus producing shRNA against CPT2. Greater than 90% of asthmatic BSM cells were effectively transduced by the lentivirus, as assessed by the percentage of GFP positive cells using flow cytometry (Supplemental figure S3A). This lentivirus significantly reduced CPT2 protein expression by 59.4 ± 3.6% in asthmatic BSM cells, as assessed by western blot analysis (Supplemental figure S3B), but it did not significantly alter CPT1 expression (Supplemental figure S3C). The specific silencing of CPT2 was shown to reduce both asthmatic (Figure 6F and G) and non-asthmatic BSM cell proliferation (Supplemental figure S4A and B), as determined by the percentage of Ki67 positive cells and by cell number. We further demonstrated that blocking LDL-R drastically decreased proliferation in

asthmatic BSM cells but not in the non-asthmatic cells (Figure 6H). We also demonstrated that etomoxir, perhexilin and the anti-LDL-R antibody did not modify asthmatic BSM cell apoptosis compared to that observed for the non-asthmatic cells (Supplemental figure S5). Moreover, blocking fatty acid entry using an LDL-R-blocking antibody or inhibiting fatty acid entry into mitochondria using etomoxir, perhexilin or dedicated lentivirus producing shRNA against CPT2 did not normalize mitochondrial mass in asthmatic BSM cells (Supplemental figure S6). Finally, we assessed the effect of optimal concentrations of steroids (*i.e.*, fluticasone, budesonide) alone or in combination with long acting-beta-2 agonists (*i.e.*, salmeterol, formoterol) on asthmatic BSM cells. None of these compounds, either alone or in combination, was able to significantly alter either CPT2 or LDL-R expression (Supplemental figure S7) or ATP production (Supplemental figure S8) in asthmatic BSM cells.

DISCUSSION

Taken together, the results of the present study demonstrate, for the first time, that hyperproliferative asthmatic BSM is characterized by a switch towards mitochondrial fatty acid metabolism both *in vitro* and *ex vivo*. Moreover, this switch is responsible for the hyperplasia observed in asthmatic BSM. Finally, 2 transport proteins implicated in this increased fatty acid metabolism were identified namely CPT2 and LDL-R, suggesting that they may represent novel therapeutic targets for asthmatic BSM remodelling.

In the present study, which initially confirmed previous findings related to the increase in mitochondrial mass and BSM cell proliferation in asthma [8], we focused on mitochondrial bioenergetics to identify specific pathways in these phenomena. In this regard, a key role of the fatty acid metabolism pathway in asthmatic BSM, both *in vitro* and *ex vivo*, was demonstrated using several complementary approaches. The first one was a metabolomic approach, using ^{13}C-labelled glucose. Metabolite production in asthmatic and non-asthmatic BSM cells was analysed, revealing a significant increase in pyruvate, succinate and malate production by asthmatic BSM cells. Consequently, ATP production was increased in asthmatic BSM cells, a finding in agreement with our previous result regarding the increase in cellular respiration within asthmatic BSM cells [8]. With respect to ROS implication in ATP production, unlike in bronchial epithelial cells, where mitochondrial dysfunction is related to increased ROS exposure causing electron transport chain subunit inhibition leading to ATP depletion [21-23], in asthmatic BSM cells, metabolic rewiring appeared independent of ROS production. Indeed, we showed that protein carbonylation was not different between non-asthmatic and asthmatic BSM cells. The second approach was based on an unbiased proteomic analyses of BSM cells. Proteome remodelling is an important aspect of cell phenotypic change [24], and we showed, here, that the major

proteome alterations occurred in clusters representative of mitochondrial and bioenergetic pathways. These findings have not been previously reported in asthmatic BSM, even though similar proteome remodelling has already been observed in cancer cells with energetic metabolism changes [25]. One could argue, however, that, such mitochondrial proteome rearrangements may be related to specific mutations of mitochondrial genes. We thus examined at GWAS databases obtained from asthmatic patients (GCST010043 and GCST009798) and identified a single mutation within the genes implicated in the mitochondrial dysfunction box (*i.e.*, ACO2, aconitase 2) [26, 27]. Indeed, ACO2 catalyses the isomerization of citrate to isocitrate within mitochondria during the TCA cycle. Specifically, the proteomic analysis revealed that palmitoyl transferase-2 (CPT2), a mitochondrial fatty acid transporter allowing fatty acids to follow the β-oxidation pathway for ATP production was the most significantly upregulated protein in asthmatic BSM cells compared to that observed in the ~~control~~ non-asthmatic BSM cells as will be discussed below. The third approach analysed the expression of the transport system of the precursor of fatty acids, namely LDL-R, which was also specifically increased in asthmatic BSM.

Fatty acid content was directly measured in BSM *in vitro* and through high resolution MALDI-mass spectrometry imaging *ex vivo*. Fatty acid consumption was increased in asthmatic BSM compared to non-asthmatic BSM in both experimental conditions. Similarly, mass spectrometry has been recently used to assess lipidome rearrangements, in colorectal cancer [14], where Mika et al. observed decreased levels of monounsaturated fatty acids (*i.e.*, oleic acid) [14]. Fatty acid oxidation occurs within mitochondria and enables cells to produce large amounts of ATP [28, 29]. Our findings, obtained using human patient samples, appeared to be restricted to BSM both

in vitro and *in vivo*, since fatty acid consumption was similar in asthmatic and non-asthmatic bronchial epithelium.

We next demonstrated a causal link between fatty acid metabolism and the proliferation of asthmatic BSM cells. Using both pharmacological and lentiviral strategies, blocking fatty acid transport decreased asthmatic BSM cell proliferation. In contrast, the use of steroids alone or in combination with LABA, was unable to decrease CPT2 or LDL-R expression or ATP production in asthmatic BSM cells. These results are in agreement with those previously published on the absence of a significant effect of steroids on asthmatic BSM cell proliferation [30]. Indeed, as the protein expression of both CPT2 and LDL-R was increased in asthmatic BSM, blockade of either CPT2 or LDL-R significantly decreased asthmatic BSM cell proliferation. CPT2, in association with its isoform CPT1, is responsible for fatty acid transport from the cytoplasm to the mitochondria, whereas LDL-R transports lipoprotein-enriched triglycerides, a major source of fatty acids, into the cytoplasm [15-17]. A similar link between fatty acid metabolism and cell proliferation has been previously demonstrated in hepatocytes [13] and cancer cells [14]. However, in our study, the effect of blocking fatty acid transport was restricted to asthmatic BSM cells, since we did not observe any effect of etomoxir or perhexilin in non-asthmatic BSM or bronchial epithelial cells. Indeed, the cancer-induced inhibition of CPT2 has been shown to be associated with an accumulation of fatty acids in the cytoplasm of hepatocellular carcinoma cells [20]. The role of LDL-R is to transport lipoprotein-enriched triglycerides, a major source of fatty acids, into the cytoplasm [21, 23, 24]. Moreover, ApoB lipoprotein and LDL levels have been shown to be negatively correlated with FEV1 in asthma, indicating a strong link between lipoprotein-enriched triglycerides and worse respiratory function in asthma [25]. LDL-R

expression is observed not only in the liver but also in various other tissues, including the lung [21, 22], and we demonstrated its expression in BSM cells.

To compare our proteomic results with previous publications, we examined at various public proteomic and RNAseq databases. Surprisingly, we did not identify any proteomic dataset and only a single RNAseq study performed on asthmatic BSM (Online dataset GSE119579) [31]. However, Fong et al. did not detect any difference in CPT2 and LDL-R mRNA expression between asthmatic and non-asthmatic BSM [31]. The discrepancy between these mRNA data and our observations of increased protein expression of both CPT2 and LDL-R in asthmatic BSM has to be related to the fact that previous studies have highlighted that the metabolic cell switch can be characterized by protein expression alterations without mRNA expression modifications [32]. Other fatty acid receptors FFAR1 and FFAR4, have been described in BSM cells [33] and associated with increased BSM cell proliferation induced by oleic and linoleic acids [34]. However, these additional fatty acid receptors and transporters were not increased in the asthmatic BSM as observed using our unbiased proteomic analyses.

In summary, BSM remodelling is a key feature of asthma pathophysiology, but no pharmacological compound has been identified that inhibits this process [7]. We previously demonstrated that blocking abnormal calcium entry within asthmatic BSM cells using gallopamil was also able to normalize BSM cell proliferation *in vitro* [8], although its effect was less impressive *in vivo* [11]. In the present study, we demonstrated that asthmatic BSM is characterized by an increased mitochondrial metabolism that specifically involves fatty acid oxidation both *in vitro* and *ex vivo* and identified 2 new targets (*i.e*., CPT2 or LDL-R). Blocking CPT2 or LDL-R dramatically decreased asthmatic BSM cell proliferation *in vitro*. Thus,

mitochondrial metabolism may represent a new target for the treatment of asthmatic BSM remodelling, although further studies are needed to elucidate the driving force responsible for metabolic remodelling in asthmatic BSM cells.

ACKNOWLEDGEMENTS

We thank the staff of the pathology and surgery departments at the University Hospital of Bordeaux as well as Isabelle Goasdoue, Benedicte Bestieu, Virginie Niel, and Marine Servat from the Clinical Investigation Center for technical assistance.

REFERENCES

1. 2020 GINA Report, Global Strategy for Asthma Management and Prevention. 2020.
2. Bara I, Ozier A, Tunon de Lara JM, Marthan R, Berger P. Pathophysiology of bronchial smooth muscle remodelling in asthma. *Eur Respir J* 2010: 36(5): 1174-1184.
3. Pepe C, Foley S, Shannon J, Lemiere C, Olivenstein R, Ernst P, Ludwig MS, Martin JG, Hamid Q. Differences in airway remodeling between subjects with severe and moderate asthma. *J Allergy Clin Immunol* 2005: 116(3): 544-549.
4. Ramos-Barbon D, Fraga-Iriso R, Brienza NS, Montero-Martinez C, Verea-Hernando H, Olivenstein R, Lemiere C, Ernst P, Hamid QA, Martin JG. T Cells localize with proliferating smooth muscle alpha-actin+ cell compartments in asthma. *Am J Respir Crit Care Med* 2010: 182(3): 317-324.
5. Girodet PO, Allard B, Thumerel M, Begueret H, Dupin I, Ousova O, Lassalle R, Maurat E, Ozier A, Trian T, Marthan R, Berger P. Bronchial Smooth Muscle Remodeling in Nonsevere Asthma. *Am J Respir Crit Care Med* 2016: 193(6): 627-633.
6. O'Reilly R, Ullmann N, Irving S, Bossley CJ, Sonnappa S, Zhu J, Oates T, Banya W, Jeffery PK, Bush A, Saglani S. Increased airway smooth muscle in preschool wheezers who have asthma at school age. *J Allergy Clin Immunol* 2013: 131(4): 1024-1032, 1032 e1021-1016.
7. Girodet PO, Ozier A, Bara I, Tunon de Lara JM, Marthan R, Berger P. Airway remodeling in asthma: new mechanisms and potential for pharmacological intervention. *Pharmacol Ther* 2011: 130(3): 325-337.
8. Trian T, Benard G, Begueret H, Rossignol R, Girodet PO, Ghosh D, Ousova O, Vernejoux JM, Marthan R, Tunon-de-Lara JM, Berger P. Bronchial smooth muscle remodeling involves calcium-dependent enhanced mitochondrial biogenesis in asthma. *J Exp Med* 2007: 204(13): 3173-3181.
9. Trian T, Allard B, Ozier A, Maurat E, Dupin I, Thumerel M, Ousova O, Gillibert-Duplantier J, Le Morvan V, Begueret H, Girodet PO, Marthan R, Berger P. Selective dysfunction of p53 for mitochondrial biogenesis induces cellular proliferation in bronchial smooth muscle from asthmatic patients. *J Allergy Clin Immunol* 2016: 137(6): 1717-1726 e1713.
10. Johnson PR, Roth M, Tamm M, Hughes M, Ge Q, King G, Burgess JK, Black JL. Airway smooth muscle cell proliferation is increased in asthma. *Am J Respir Crit Care Med* 2001: 164(3): 474-477.
11. Girodet PO, Dournes G, Thumerel M, Begueret H, Dos Santos P, Ozier A, Dupin I, Trian T, Montaudon M, Laurent F, Marthan R, Berger P. Calcium Channel Blocker Reduces Airway Remodeling in Severe Asthma: a Proof-of-concept Study. *Am J Respir Crit Care Med* 2015.
12. Rohrig F, Schulze A. The multifaceted roles of fatty acid synthesis in cancer. *Nat Rev Cancer* 2016: 16(11): 732-749.
13. Berge RK, Garras A, Asins G, Serra D, Hegardt FG, Madsen L. Mitochondrial 3-hydroxy-3-methylglutaryl CoA synthase and carnitine palmitoyltransferase II are potential control sites of hepatic ketogenesis under conditions of peroxisome proliferation. *Lipids* 1999: 34 Suppl: S163.
14. Mika A, Kobiela J, Pakiet A, Czumaj A, Sokolowska E, Makarewicz W, Chmielewski M, Stepnowski P, Marino-Gammazza A, Sledzinski T. Preferential uptake of polyunsaturated fatty acids by colorectal cancer cells. *Sci Rep* 2020: 10(1): 1954.
15. Herz J, Bock HH. Lipoprotein receptors in the nervous system. *Annu Rev Biochem* 2002: 71: 405-434.

16. Dieckmann M, Dietrich MF, Herz J. Lipoprotein receptors--an evolutionarily ancient multifunctional receptor family. *Biol Chem* 2010: 391(11): 1341-1363.
17. Botham KM, Wheeler-Jones CP. Postprandial lipoproteins and the molecular regulation of vascular homeostasis. *Prog Lipid Res* 2013: 52(4): 446-464.
18. Bara I, Ozier A, Girodet PO, Carvalho G, Cattiaux J, Begueret H, Thumerel M, Ousova O, Kolbeck R, Coyle AJ, Woods J, Tunon de Lara JM, Marthan R, Berger P. Role of YKL-40 in bronchial smooth muscle remodeling in asthma. *Am J Respir Crit Care Med* 2012: 185(7): 715-722.
19. Henriet E, Abou Hammoud A, Dupuy JW, Dartigues B, Ezzoukry Z, Dugot-Senant N, Leste-Lasserre T, Pallares-Lupon N, Nikolski M, Le Bail B, Blanc JF, Balabaud C, Bioulac-Sage P, Raymond AA, Saltel F. Argininosuccinate synthase 1 (ASS1): A marker of unclassified hepatocellular adenoma and high bleeding risk. *Hepatology* 2017: 66(6): 2016-2028.
20. Bochner BR, Gadzinski P, Panomitros E. Phenotype microarrays for high-throughput phenotypic testing and assay of gene function. *Genome Res* 2001: 11(7): 1246-1255.
21. Aguilera-Aguirre L, Bacsi A, Saavedra-Molina A, Kurosky A, Sur S, Boldogh I. Mitochondrial dysfunction increases allergic airway inflammation. *J Immunol* 2009: 183(8): 5379-5387.
22. Mabalirajan U, Dinda AK, Kumar S, Roshan R, Gupta P, Sharma SK, Ghosh B. Mitochondrial structural changes and dysfunction are associated with experimental allergic asthma. *J Immunol* 2008: 181(5): 3540-3548.
23. Huttemann M, Lee I, Gao X, Pecina P, Pecinova A, Liu J, Aras S, Sommer N, Sanderson TH, Tost M, Neff F, Aguilar-Pimentel JA, Becker L, Naton B, Rathkolb B, Rozman J, Favor J, Hans W, Prehn C, Puk O, Schrewe A, Sun M, Hofler H, Adamski J, Bekeredjian R, Graw J, Adler T, Busch DH, Klingenspor M, Klopstock T, Ollert M, Wolf E, Fuchs H, Gailus-Durner V, Hrabe de Angelis M, Weissmann N, Doan JW, Bassett DJ, Grossman LI. Cytochrome c oxidase subunit 4 isoform 2-knockout mice show reduced enzyme activity, airway hyporeactivity, and lung pathology. *FASEB J* 2012: 26(9): 3916-3930.
24. Bruce C, Stone K, Gulcicek E, Williams K. Proteomics and the analysis of proteomic data: 2013 overview of current protein-profiling technologies. *Curr Protoc Bioinformatics* 2013: Chapter 13: Unit 13 21.
25. Caro P, Kishan AU, Norberg E, Stanley IA, Chapuy B, Ficarro SB, Polak K, Tondera D, Gounarides J, Yin H, Zhou F, Green MR, Chen L, Monti S, Marto JA, Shipp MA, Danial NN. Metabolic signatures uncover distinct targets in molecular subsets of diffuse large B cell lymphoma. *Cancer Cell* 2012: 22(4): 547-560.
26. Han Y, Jia Q, Jahani PS, Hurrell BP, Pan C, Huang P, Gukasyan J, Woodward NC, Eskin E, Gilliland FD, Akbari O, Hartiala JA, Allayee H. Genome-wide analysis highlights contribution of immune system pathways to the genetic architecture of asthma. *Nat Commun* 2020: 11(1): 1776.
27. Olafsdottir TA, Theodors F, Bjarnadottir K, Bjornsdottir US, Agustsdottir AB, Stefansson OA, Ivarsdottir EV, Sigurdsson JK, Benonisdottir S, Eyjolfsson GI, Gislason D, Gislason T, Guethmundsdottir S, Gylfason A, Halldorsson BV, Halldorsson GH, Juliusdottir T, Kristinsdottir AM, Ludviksdottir D, Ludviksson BR, Masson G, Norland K, Onundarson PT, Olafsson I, Sigurdardottir O, Stefansdottir L, Sveinbjornsson G, Tragante V, Gudbjartsson DF, Thorleifsson G, Sulem P, Thorsteinsdottir U, Norddahl GL, Jonsdottir I, Stefansson K. Eighty-eight variants highlight the role of T cell regulation and airway remodeling in asthma pathogenesis. *Nat Commun* 2020: 11(1): 393.

28. Vazquez A, Kamphorst JJ, Markert EK, Schug ZT, Tardito S, Gottlieb E. Cancer metabolism at a glance. *J Cell Sci* 2016: 129(18): 3367-3373.
29. Vander Heiden MG, Cantley LC, Thompson CB. Understanding the Warburg effect: the metabolic requirements of cell proliferation. *Science* 2009: 324(5930): 1029-1033.
30. Roth M, Johnson PR, Borger P, Bihl MP, Rudiger JJ, King GG, Ge Q, Hostettler K, Burgess JK, Black JL, Tamm M. Dysfunctional interaction of C/EBPalpha and the glucocorticoid receptor in asthmatic bronchial smooth-muscle cells. *N Engl J Med* 2004: 351(6): 560-574.
31. Fong V, Hsu A, Wu E, Looney AP, Ganesan P, Ren X, Sheppard D, Wicher SA, Thompson MA, Britt RD, Jr., Prakash YS, Bhattacharya M. Arhgef12 drives IL17A-induced airway contractility and airway hyperresponsiveness in mice. *JCI Insight* 2018: 3(21).
32. Zhang B, Wang J, Wang X, Zhu J, Liu Q, Shi Z, Chambers MC, Zimmerman LJ, Shaddox KF, Kim S, Davies SR, Wang S, Wang P, Kinsinger CR, Rivers RC, Rodriguez H, Townsend RR, Ellis MJ, Carr SA, Tabb DL, Coffey RJ, Slebos RJ, Liebler DC, Nci C. Proteogenomic characterization of human colon and rectal cancer. *Nature* 2014: 513(7518): 382-387.
33. Mizuta K, Zhang Y, Mizuta F, Hoshijima H, Shiga T, Masaki E, Emala CW, Sr. Novel identification of the free fatty acid receptor FFAR1 that promotes contraction in airway smooth muscle. *Am J Physiol Lung Cell Mol Physiol* 2015: 309(9): L970-982.
34. Matoba A, Matsuyama N, Shibata S, Masaki E, Emala CW, Sr., Mizuta K. The free fatty acid receptor 1 promotes airway smooth muscle cell proliferation through MEK/ERK and PI3K/Akt signaling pathways. *Am J Physiol Lung Cell Mol Physiol* 2018: 314(3): L333-L348.

Table 1: Clinical characteristics of all subjects

Characteristics	Non-asthmatic subjects	Asthmatic patients	P Values
No. of patients	31	21	NS
Age (yr)	65 ± 8	55 ± 16	NS
Sex ratio (M/F)	17/14	6/15	NS
BMI (kg/m^2)	24.9± 5.0	25.9 ± 5.4	NS
Smoking history			
Pack years	36.3 ± 21.8	1.9 ± 2.9	0.0001
Current (no. of patients/total of patients)	13/31	0/21	0.0006
Former (no. of patients/total of patients)	12/31	8/21	NS
Treatments			
ICS (Yes/No)	0/31	21/0	< 0.0001
LABA (Yes/No)	0/31	20/1	< 0.0001
OCS (Yes/No)	0/31	3/18	NS
FEV_1			
Liters	2.47 ± 0.85	1.97 ± 0.68	0.03
Percentage of predicted value	89.3 ± 22.2	75.8 ± 22.7	0.03
FEV_1: FVC ratio	0.74 ± 0.12	0.71 ± 0.10	NS

FVC				
	Liters	3.37 ± 1.15	2.78 ± 0.77	0.04
	Percentage of predicted value	99.2 ± 19.8	89.9 ± 20.4	NS
FeNO				
	ppb	ND	32.8 ± 26	

Data are presented as the mean ± SD for continuous normal variables. Comparisons of continuous variables was made using either Mann-Whitney or t-tests. Categorical variables were analysed using Fisher's exact tests.

BMI= body mass index; ICS= inhaled corticosteroids; LABA= long-acting beta2-agonist; M/F=male/female; OCS: oral corticosteroid; FEV_1= forced expiratory volume in one second, FVC= forced volume capacity; FeNO= fractional exhaled nitric oxide; ppb: parts per billion; NS = not significant; ND = not determined.

FIGURE LEGENDS

Figure 1: Increased asthmatic BSM cell proliferation is associated with mitochondrial mass

(A) Growth curves of non-asthmatic (white circles, n=12) and asthmatic (black squares, n=10) BSM cells were obtained by performing cell counting at 72 hours. ** P<0.01 using two-way ANOVA statistical test. Cell proliferation was assessed by **(B)** BrdU incorporation assay (n=9) or **(C)** Ki67 staining and flow cytometry (n=6), using non-asthmatic (white circles) and asthmatic (black squares) BSM cells. * P<0.05 using Mann-Whitney statistical test. **(D)** Levels of basal apoptosis (-) and induced apoptosis (+) using 100 µM tert-butyl-hydroxide (TBHP) for 1 hour were analysed by measuring caspase 3 and 7 activities and bioluminescent assays. ** P<0.01 and *** P<0.001 using one-way ANOVA statistical test**. (E)** Immunoblot detection of 2,4-dinitrophenylhydrazine (DNPH) carbonyl groups using whole-cell lysates of non-asthmatic (white circles, n=4) and asthmatic (black squares, n=4) BSM cells normalized by β-actin content. * P<0.05 using Mann-Whitney statistical test. **(F)** Representative mitochondrial networks and quantification were obtained by immunofluorescence imaging of TOMM20 in non-asthmatic (white circles, n=4) and asthmatic BSM cells (black squares, n=4). Immunoblot analysis of mitochondrial mass markers, including porin (**G**, n=4), citrate synthase (**H**, n=4) and TOMM20 (**I**, n=4) protein expression levels in non-asthmatic (white circles) and asthmatic (black squares) BSM cells. * P<0.05, using Mann-Whitney statistical test. Stain free gel technology was used for loading control expression quantification. Data are presented as the mean ± SEM (A) or dot plots with the median (B-I).

Figure 2: Increased energy metabolism is observed in asthmatic BSM cells

(A) Oxygen consumption rate (OCR) was measured in different respiratory states: basal (DMEM 5 mM glucose), leak (30 µM oligomycin), and maximal (MAX, 5 µM CCCP), in non-asthmatic

(white circles, n=16) and asthmatic (black squares, n=15) BSM cells. Reserve capacity (RES CAP) was calculated as the difference between the maximal and basal respiratory rates. The different rates were corrected for non-mitochondrial respiration determined after the addition of 1 mM potassium cyanide. * P<0.05, and *** P<0.001 using two-way ANOVA statistical test. **(B)** Steady-state ATP content was measured in non-asthmatic (white circles, n=12) and asthmatic (black squares, n=8) BSM cells using a luminescence assay. **(C)** The portion of ATP produced by mitochondria in asthmatic BSM cells was inhibited using a cocktail of OXPHOS inhibitors (see 'Methods') (n=8). Metabolomics was performed using ^{13}C-mass spectrometry analysis of **(D)** pyruvate, **(E)** succinate and **(F)** malate peak intensity in non-asthmatic (white circles, n=5) and asthmatic (black squares, n=5) BSM cells. **(G)** Resting glucose and **(H)** lactate production concentrations were assessed in the culture medium of non-asthmatic (white circles, n=12) and asthmatic (black squares, n=10) BSM cells. **(I)** Steady-state ATP content in non-asthmatic (white circles, n=5) and asthmatic (black squares, n=5) BSM cells using ^{13}C-mass spectrometry. Data are presented as dot plots with the median. * P<0.05, using Mann-Whitney statistical test.

Figure 3: Proteome remodelling promotes bioenergetics in asthmatic BSM

(A) Proteome comparison between non-asthmatic and asthmatic BSM cells *in vitro* (n=5) using ingenuity pathway analysis (IPA) from the raw proteomic data. Proteins with a different expression levels were organized based on pre-defined categories suggested by IPA. Then, the proteins with different expression levels were assigned to these IPA categories based on the IPA database. Categories were ranked according to their frequency of identification in the proteome [-log (p value)]. **(B)** Volcano plots of differentially expressed genes in the non-asthmatic (n=5) and asthmatic (n=5) BSM cells using mass spectrometry analysis. Y axis line at y= 1.3 represents

p=0.05. The red dot represents CPT2. **(C)** Immunoblot of CPT2 protein expression in non-asthmatic (white circles, n=7) and asthmatic (black squares, n=7) BSM cells. Stain free gel technology was used for loading control expression quantification. Data are presented as dot plots with the median. * $p < 0.05$, using Mann-Whitney statistical test.

Figure 4: Fatty acid uptake is increased in asthmatic BSM cells

(A) Immunoblot of LDL-R protein expression in non-asthmatic (white circles, n=7) and asthmatic (black squares, n=7) BSM cells. Stain free gel technology was used for loading control expression quantification. **(B)** Representative images of incorporated fluorescent ceramide (green) in non-asthmatic and asthmatic BSM cells. Nuclei were stained in blue with DAPI. **(C)** Quantification of endocytosis of fluorescent ceramide 20 min after its addition to the cell culture medium in non-asthmatic (white circles, n=5) and asthmatic (black squares, n=5) BSM cells. Fluorescence was normalized to cell number. Data are expressed above the mean non-asthmatic value. **(D)** Incorporation of fluorescent ceramide was measured by fluorimetry in non-asthmatic (white circles, n=4) and asthmatic (black squares, n=4) BSM cells. A.U indicates arbitrary unit. **(E)** Free fatty acid (FFA) resting concentration in the medium of non-asthmatic (white circles, n=7) and asthmatic (black squares, n=7) BSM cells was measured by absorbance (OD). **(F)** Palmitoyl-D,L-carnitine reduction of cytochrome c using Biolog assay in non-asthmatic (white circles, n=4) and asthmatic (black squares, n=4) BSM cells. Data are presented as dot plots with the median. * $p < 0.05$, using Mann-Whitney statistical test.

Figure 5: *Ex vivo* demonstration of fatty acid consumption by asthmatic BSM

Arachidonate **(A and E)**, stearate **(B and F)**, linoleate **(C and G)** and palmitate **(D and H)** levels were quantified in bronchial smooth muscle (BSM) and in bronchial epithelium (BE) from non-asthmatic (white circles, n=6) and asthmatic (black squares, n=7) biopsies using MALDI-mass spectrometry imaging analysis. Data are presented as dot plots with the median. * $p < 0.05$, using Mann-Whitney statistical test. NS indicates non-significant. A.U indicates arbitrary unit.

Figure 6: Blocking fatty acid oxidation dramatically decreases asthmatic BSM cell proliferation

(A) Growth curves of non-asthmatic (white circles, n=6) and asthmatic (black squares, n=6) BSM cells were obtained by performing cell counting with (dotted line) or without (plain line) 10 nM etomoxir for 72 hours (two-way ANOVA). **(B)** BrdU incorporation assay in non-asthmatic (white circles, n=10) and asthmatic (black squares, n=10) BSM cells with (+) or without (-) 10 nM etomoxir for 24 hours (one-way ANOVA). **(C)** Growth curves of non-asthmatic (white circles, n=6) and asthmatic (black squares, n=6) BSM cells were obtained by performing cell counting with (dotted line) or without (plain line) 10 nM perhexilin for 72 hours (two-way ANOVA). **(D)** BrdU incorporation assay of non-asthmatic (white circles, n=10) and asthmatic (black squares, n=10) BSM cells with (+) or without (-) 10 nM perhexilin for 24 hours (one-way ANOVA). **(E)** Oxygen consumption rates (OCR) were measured under basal conditions (DMEM 5 mM glucose) with (+) or without (-) 10 nM etomoxir or 10 nM perhexilin. BSM cells were obtained from non-asthmatic (white circles, n=4) and asthmatic patients (black squares, n=4) (two-way ANOVA). Cell proliferation was assessed in asthmatic BSM cells (n=3) transduced with either a scramble shRNA lentivirus (-) or a CPT2 shRNA lentivirus (+), by Ki67

positive staining using flow cytometry **(F)** and cell counting **(G)** (Wilcoxon test). **(H)** Cell counting of non-asthmatic (white circles, n=7) and asthmatic (black squares, n=7) BSM cells cultured in the presence (+) or in the absence (-) of blocking antibody against LDL-R (one-way ANOVA). Data are presented as dot plots with the median. # Indicates the p-value between non-asthmatic and asthmatic patients (# $P<0.05$, ## $P<0.01$, ### $P<0.001$). * Indicates the p-value between groups with and without treatment (* $P<0.05$, ** $P<0.01$, *** $P<0.001$).

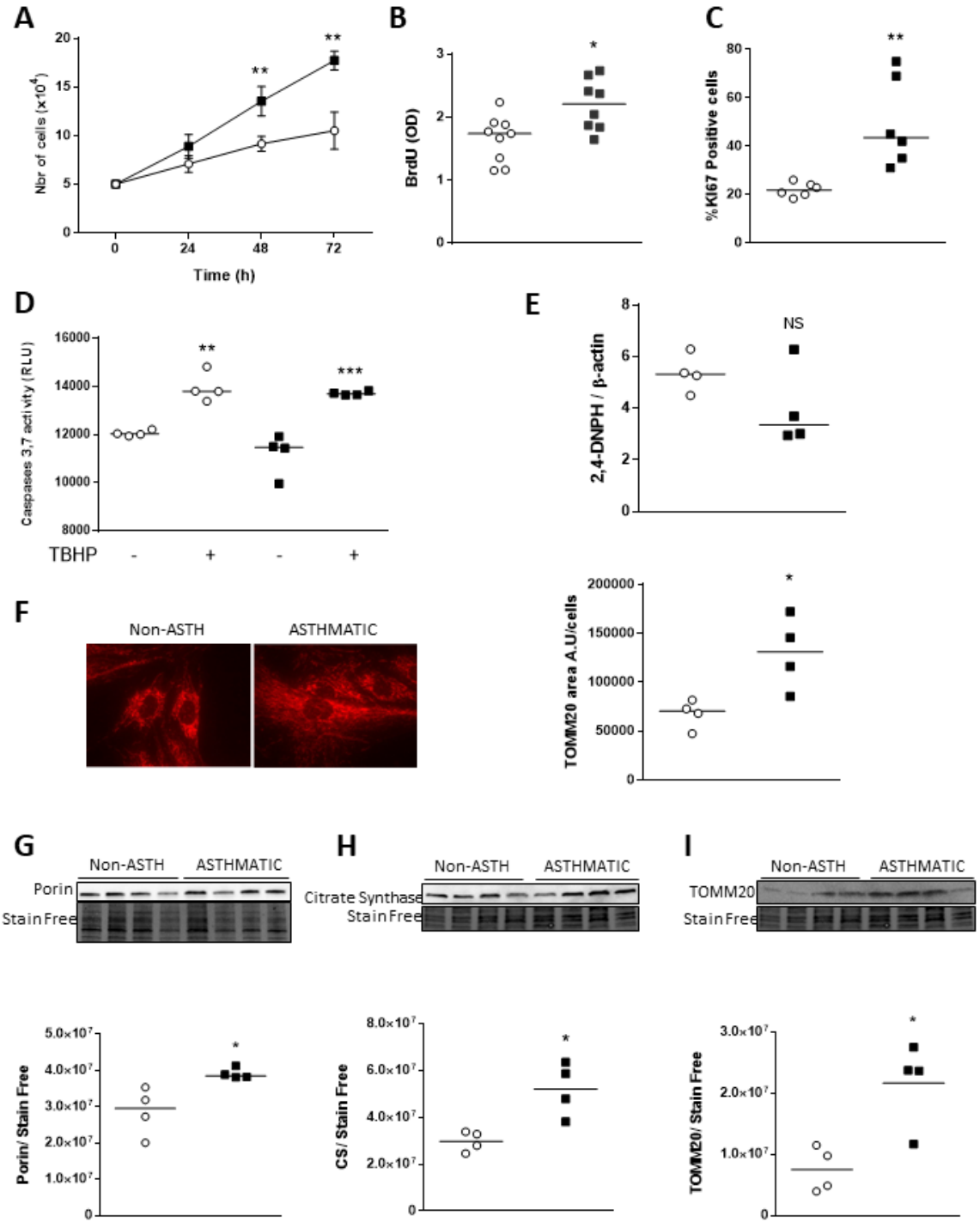
A
Nbr of cells (x10⁴)
Time (h)
B
BrdU (OD)
C
%KI67 Positive cells
D
Caspases 3,7 activity (RLU)
TBHP
E
2,4-DNPH / β-actin
NS
TOMM20 area A.U/cells
F
Non-ASTH
ASTHMATIC
G
Porin
Stain Free
Porin/ Stain Free
H
Citrate Synthase
CS/ Stain Free
I
TOMM20
TOMM20/ Stain Free

Figure 1

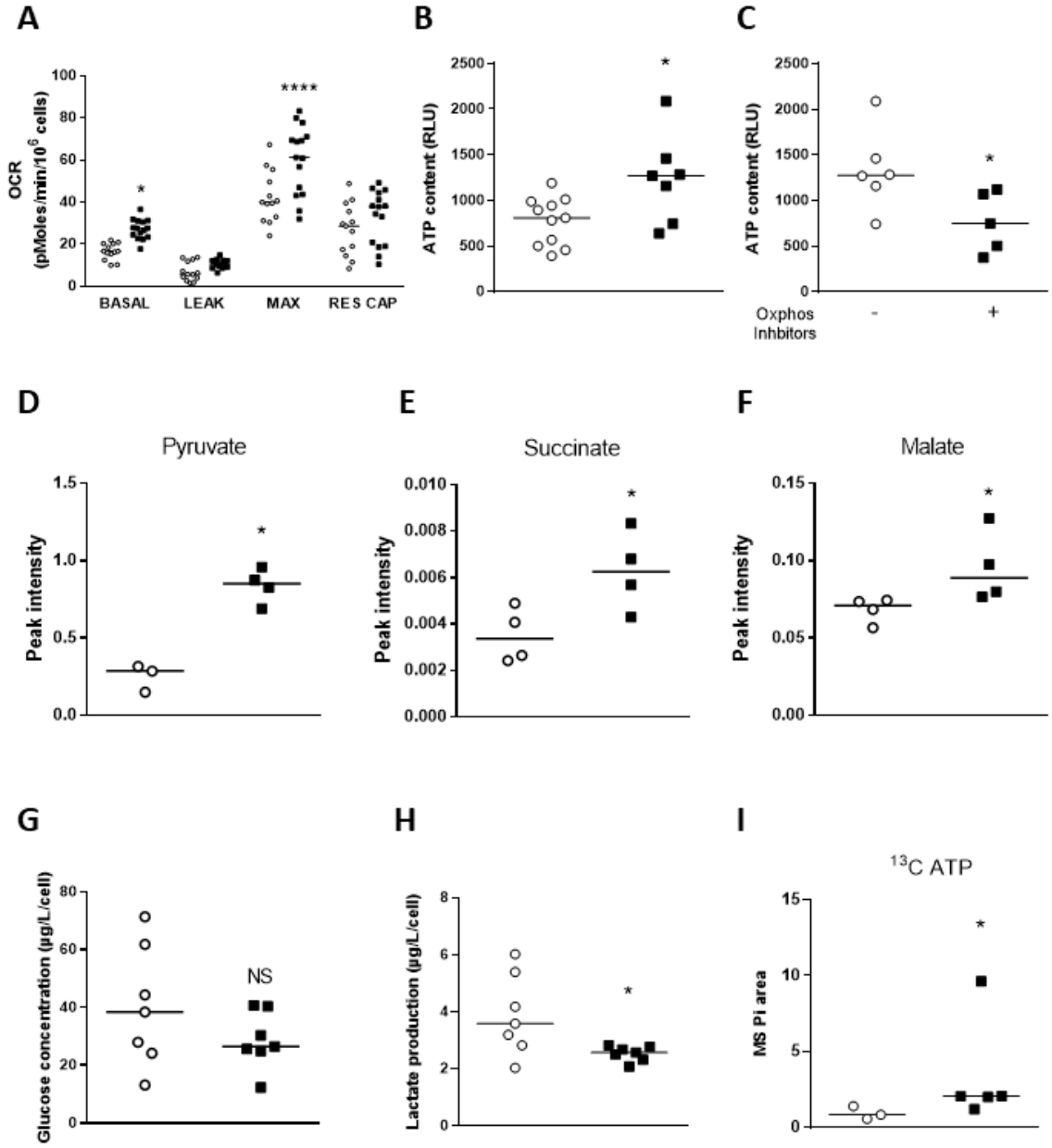
A
OCR (pMoles/min/10^6 cells)
BASAL
LEAK
MAX
RES CAP
****
B
ATP content (RLU)
C
ATP content (RLU)
Oxphos Inhbitors
D
Pyruvate
Peak intensity
E
Succinate
Peak intensity
F
Malate
Peak intensity
G
Glucose concentration (µg/L/cell)
NS
H
Lactate production (µg/L/cell)
I
13C ATP
MS Pi area

Figure 2

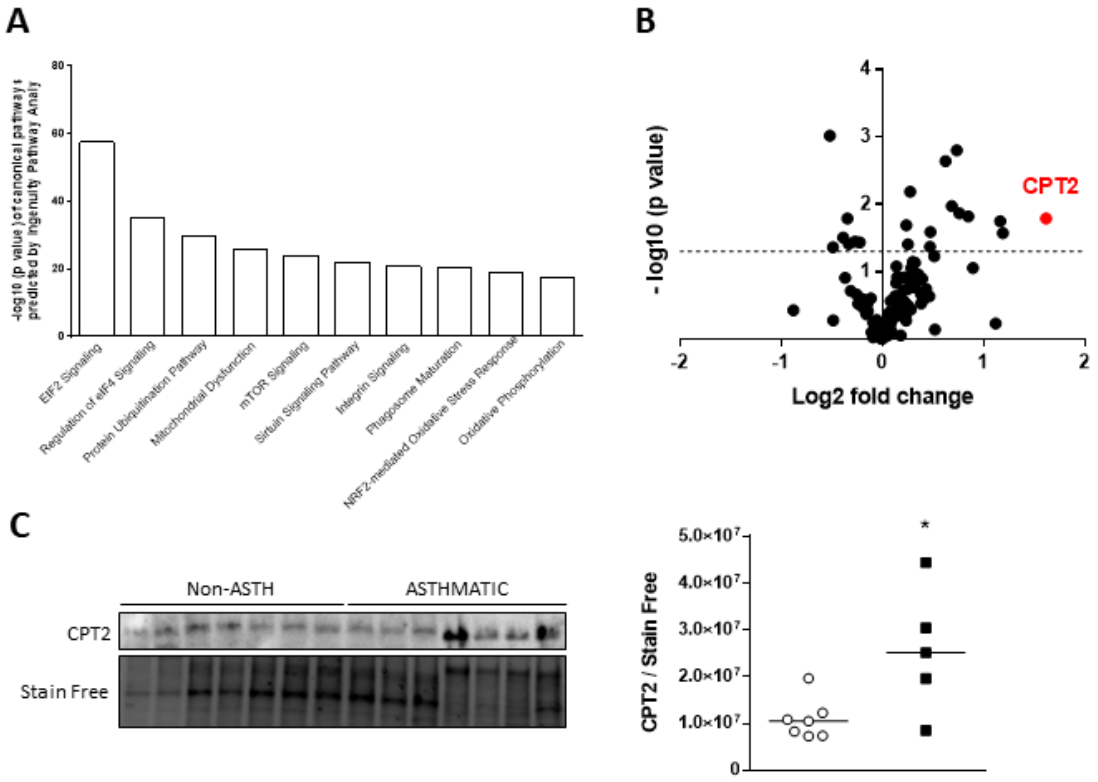
A
-log10 (p value) of canonical pathways predicted by Ingenuity Pathway Analy
80
60
40
20
0
EIF2 Signaling
Regulation of eIF4 Signaling
Protein Ubiquitination Pathway
Mitochondrial Dysfunction
mTOR Signaling
Sirtuin Signaling Pathway
Integrin Signaling
Phagosome Maturation
NRF2-mediated Oxidative Stress Response
Oxidative Phosphorylation
B
- log10 (p value)
Log2 fold change
CPT2
C
Non-ASTH
ASTHMATIC
CPT2
Stain Free
CPT2 / Stain Free
5.0×10⁷
4.0×10⁷
3.0×10⁷
2.0×10⁷
1.0×10⁷
0
*

Figure 3

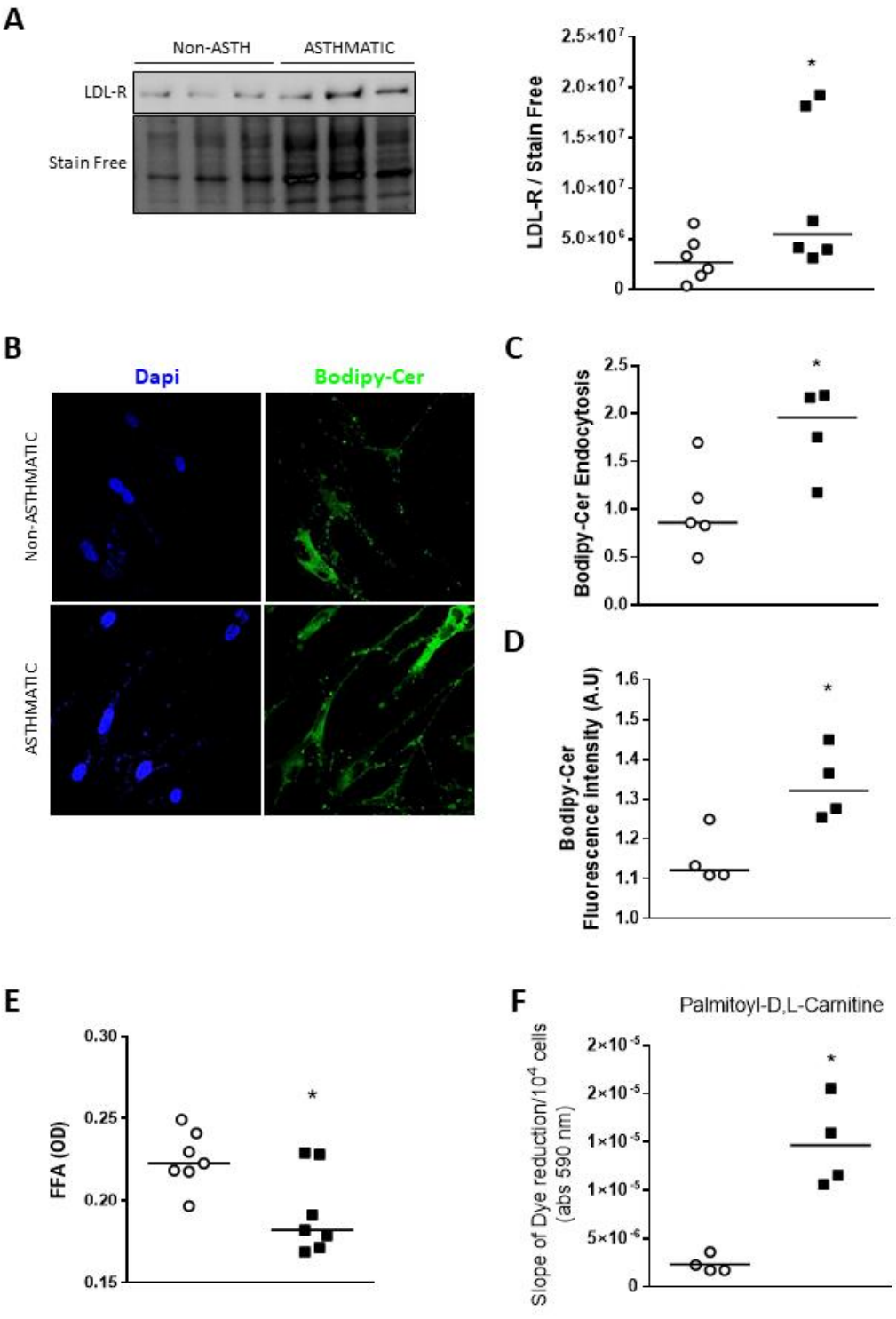
A
Non-ASTH
ASTHMATIC
LDL-R
Stain Free
LDL-R / Stain Free
2.5×10⁷
2.0×10⁷
1.5×10⁷
1.0×10⁷
5.0×10⁶
0
*
B
Dapi
Bodipy-Cer
Non-ASTHMATIC
ASTHMATIC
C
Bodipy-Cer Endocytosis
2.5
2.0
1.5
1.0
0.5
0.0
*
D
Bodipy-Cer Fluorescence Intensity (A.U)
1.6
1.5
1.4
1.3
1.2
1.1
1.0
*
E
FFA (OD)
0.30
0.25
0.20
0.15
*
F
Palmitoyl-D,L-Carnitine
Slope of Dye reduction/10⁴ cells (abs 590 nm)
2×10⁻⁵
2×10⁻⁵
1×10⁻⁵
1×10⁻⁵
5×10⁻⁶
0
*

Figure 4

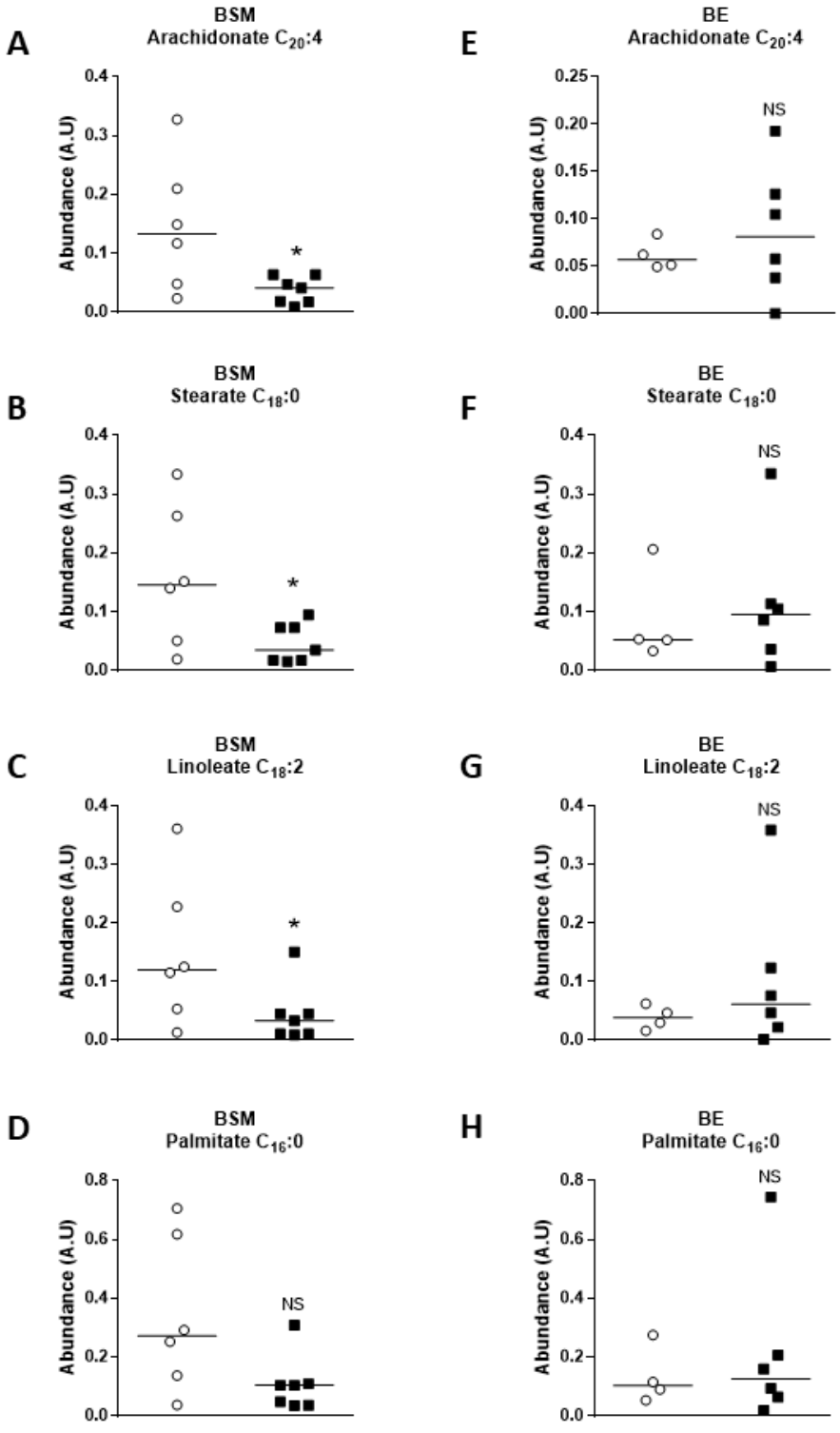
A
BSM
Arachidonate C20:4
Abundance (A.U)
0.4
0.3
0.2
0.1
0.0
*
E
BE
Arachidonate C20:4
Abundance (A.U)
0.25
0.20
0.15
0.10
0.05
0.00
NS
B
BSM
Stearate C18:0
Abundance (A.U)
0.4
0.3
0.2
0.1
0.0
*
F
BE
Stearate C18:0
Abundance (A.U)
0.4
0.3
0.2
0.1
0.0
NS
C
BSM
Linoleate C18:2
Abundance (A.U)
0.4
0.3
0.2
0.1
0.0
*
G
BE
Linoleate C18:2
Abundance (A.U)
0.4
0.3
0.2
0.1
0.0
NS
D
BSM
Palmitate C16:0
Abundance (A.U)
0.8
0.6
0.4
0.2
0.0
NS
H
BE
Palmitate C16:0
Abundance (A.U)
0.8
0.6
0.4
0.2
0.0
NS

Figure 5

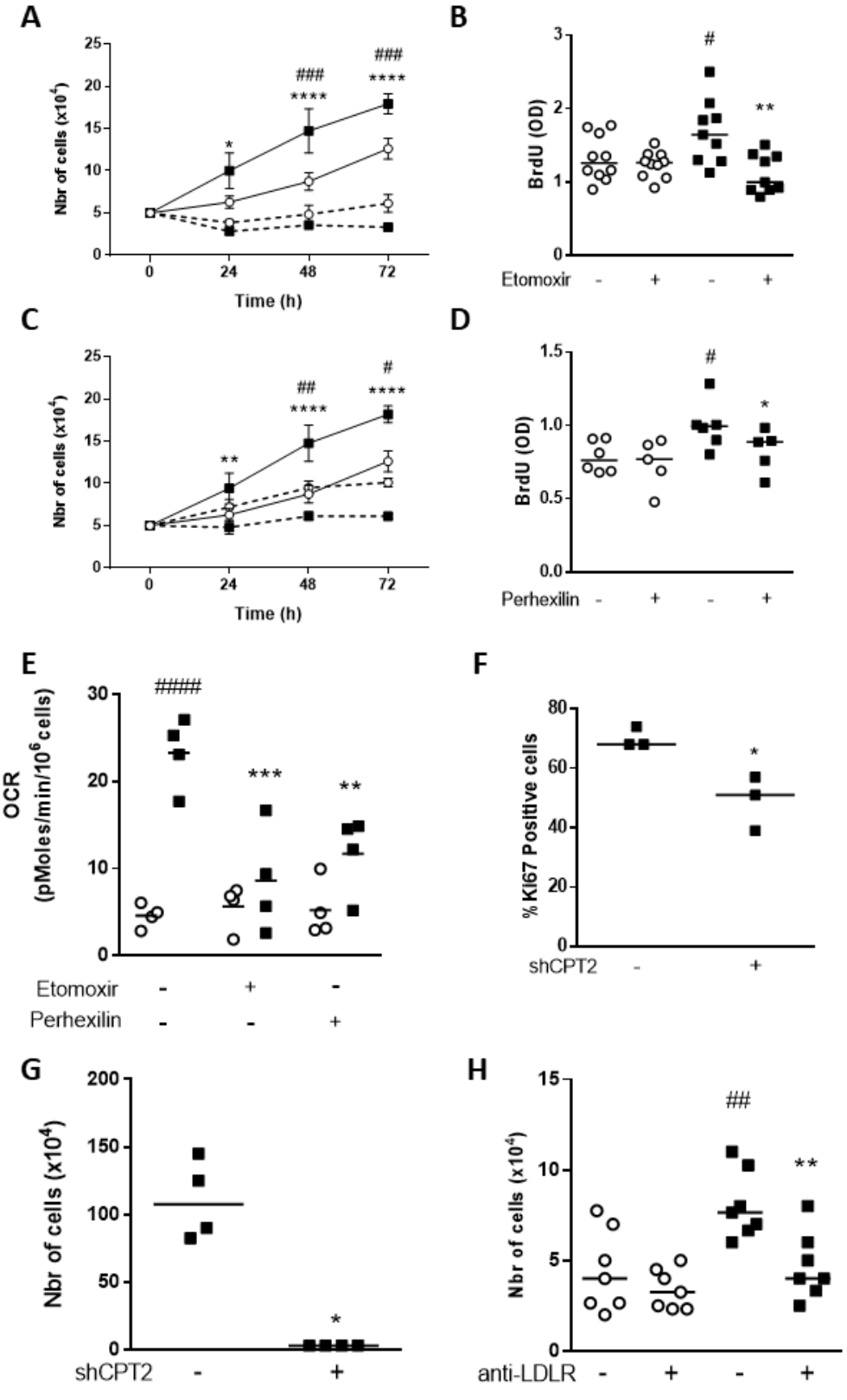
A
Nbr of cells (x10⁴)
Time (h)
B
BrdU (OD)
Etomoxir
C
Nbr of cells (x10⁴)
Time (h)
D
BrdU (OD)
Perhexilin
E
OCR
(pMoles/min/10⁶cells)
Etomoxir
Perhexilin
F
% KI67 Positive cells
shCPT2
G
Nbr of cells (x10⁴)
shCPT2
H
Nbr of cells (x10⁴)
anti-LDLR

Figure 6

SUPPLEMENTAL MATERIAL & METHODS

Crucial role of fatty acid oxidation in asthmatic bronchial smooth muscle remodeling

Pauline Esteves[1,2], Landry Blanc[1,4], Alexis Celle[1,2], Isabelle Dupin[1,2], Elise Maurat[1,2], Nivea Amoedo[1,2], Guillaume Cardouat[1,2], Olga Ousova[1,2], Lara Gales[5], Florian Bellvert[5], Hugues Begueret[3], Matthieu Thumerel[1,2,3], Jean-William Dupuy[1,4], Nicolas Desbenoit[1,4], Roger Marthan[1,2,3], Pierre-Olivier Girodet[1,2,3], Rodrigue Rossignol[1,2], Patrick Berger[1,2,3*] and Thomas Trian[1,2*]

AFFILIATIONS

[1] Univ-Bordeaux, Centre de Recherche Cardio-thoracique de Bordeaux, U1045, MRGM, Functional Genomics Center (CGFB), CIC 1401, CELLOMET, F-33000 Bordeaux, France.

[2] INSERM, Centre de Recherche Cardio-thoracique de Bordeaux, U1045, U1211, CIC 1401, F-33000 Bordeaux, France.

[3] CHU de Bordeaux, Service d'exploration fonctionnelle respiratoire, Service de chirurgie thoracique, Service d'anatomopathologie, CIC 1401, Bordeaux, France

[4] CNRS, UMR5248, Institute of Chemistry & Biology of Membranes & Nano objects, Functional Genomics Center (CGFB), Proteomics Facility, Université de Bordeaux, 33000 Bordeaux, France

[5] Université de Toulouse, CNRS 5504, INRA 792, INSA Toulouse, Toulouse Biotechnology Institute, Bio & Chemical Engineering, MetaToul, Toulouse, France

* Co-last author

MATERIALS AND METHODS

Study population

A total of 21 patients with asthma and 31 non asthmatic subjects were prospectively recruited from the "Centre Hospitalier Universitaire (CHU)" of Bordeaux, France, according to the Global Initiative for Asthma [1] and the American Thoracic Society criteria [2]. Asthmatic patients were recruited from the "COBRA" cohort (COhort of BRonchial obstruction and Asthma, ethics committee number: 2008-A00294-51/1) in the Clinical Investigation Center of Bordeaux (CIC, Hôpital Haut-Lévêque, Pessac, France). Non asthmatic control subjects were recruited after surgical resection. This study received approval from the local and national ethics committees. Bronchial specimens from all subjects were obtained by either fiberoptic bronchoscopy or lobectomy in macroscopically normal areas, as previously described [3].

Cell culture

Bronchial smooth muscle (BSM) cells were obtained from patient biopsies and bronchi dissected out from lobectomy, as previously described [4]. Briefly, BSM cell culture was performed in DMEM 25 mM glucose (Gibco, Thermo Fisher Scientific, Waltham, MA), supplemented with 10% FBS (Gibco) and penicillin-streptomycin-amphotericin B 1X (100X; Gibco) and essential amino acids 1X (100X; Sigma-Aldrich, Saint-Louis, MO). The smooth muscle phenotype was confirmed by immunocytochemistry using the double staining of smooth muscle alpha-actin and calponin. Etomoxir and perhexilin were both purchased from Sigma-Aldrich and used at 10 nM each. Blocking anti-LDL-R antibody was purchased from Sigma and used at 5 µg/mL. Salmeterol, formoterol, fluticasone and budesonide were purchased from Sigma-Aldrich and used at concentrations of 10^{-7}M, 10^{-8}M or 10^{-9}M.

Bronchial epithelial cell culture was established from bronchial brushings patients' biopsies and bronchi dissected out from lobectomy, as previously described in Trian et al. [5], using PneumaCult medium (Stemcell, Vancouver, Canada).

Lentiviral infection for genetic inhibition of CPT2 expression

BSM cells were transduced with shRNA targeted against CPT2 or negative control (scrambled shRNA) at an MOI of 20. Lenti shRNA were purchased from Origene. Lentiblast (OZ Biosciences, San Diego, CA) was used as a transduction reagent following the manufacturer's recommendations. Knock-down was effective after 5 days of treatment as assessed by western blot.

Cellular oxygen consumption rate

Cellular oxygen consumption rate (OCR) was measured in intact cells at 37°C in a 2 mL thermostatically monitored chamber (1.0×10^6 cells/ml /run) using an Oroboros O2k instrument (Oroboros Instruments, Innsbruck, Austria). High-resolution respirometry was determined under routine conditions (in DMEM), in the presence of 6 μM oligomycin (leak respiration independent of ADP phosphorylation), or in the presence of 8 μM carbonyl-cyanide m-chlorophenylhydrazone CCCP (maximal respiration obtained in the uncoupled state). The 'reserve capacity' corresponds to the difference between the maximal respiration (CCCP-stimulated) and the basal respiration obtained in the cell culture medium. Finally, the cellular non-mitochondrial respiration was obtained after inhibition of the respiratory chain using potassium cyanide (KCN).

Cellular and mitochondrial ATP synthesis

Steady-state ATP content was measured by bioluminescence using the CellTiter Glo kit (Promega, Madison, WI), following the manufacturer's recommendations. The OXPHOS inhibitory cocktail contained 30 µM oligomycin, 5 µM rotenone and 1 mM potassium cyanide. ATP content was normalized to crystal violet staining representing cell density obtained at 570 nm.

Oxidative stress

Oxyblots were performed on total cellular lysates using an OxyBlot protein detection kit (Merck Millipore, Burlington, MA) and 2,4-dinitrophenylhydrazine (2,4-DNPH) antibody.

Cell culture substrates concentration measurement

Free fatty acid resting concentration in the cell culture medium was analysed after 48 hours following the manufacturer's recommendations from Abnova (Taipei, Taïwan). Both glucose and lactate concentrations were measured in the cell culture medium using a YSI Biochemistry Analyzer.

Metabolites analysis by IC-MS/MS

BSM cells were incubated in DMEM without glucose (Life Invitrogen, Thermo Fisher Scientific) supplemented with 25 mM of [U-^{13}C]-glucose (Sigma-Aldrich) for 48 hours before fast filtration preparation of the samples for mass spectrometry analysis. Extraction and quenching of metabolites were performed using a specific protocol from Metatoul (Metatoul,

Toulouse, France) as previously described by Heuillet M. et al. Metabolites were analysed by ionic-exchange chromatography coupled with tandem mass spectrometry (IC-MS/MS) using a previously described method [6].

Fatty acids endocytosis

BSM cells were seeded at 10 000 cells in 8 well chamber slides. BSM cells were rapidly starved of FBS and incubated for 30 min in DMEM medium without FBS. Fluorescent BODIPY-ceramide was purchased from Life Invitrogen (Thermo Fisher Scientific) and used at 100 ug/mL following the manufacturer's recommendations. DAPI was used for nuclear staining.

Metabolic capability analysis – Biolog phenotype MicroArrays

About 20 000 asthmatic and control BSM cells were seeded into 96-well MitoPlate^{TM} S-1 and MitoPlate^{TM} I-1 BIOLOG plates. The metabolic capability of cells was assessed via redox reactions associated with cellular respiration following the manufacturer's instructions (Biolog, Hayward, CA).

Cell proliferation assays

For cell quantification, cells were trypsinized and counted at different time points. A BrdU cell proliferation colorimetric kit (Abcam, Cambridge, UK) was used following the manufacturer's instructions. BSM cells positive for Ki67 staining were analysed by flow cytometry.

Mitochondrial network immunostaining

BSM cells were seeded into Nunc Lab-Tek chamber slides at 5000 cells per chamber. TOMM20 was used for mitochondrial network staining and visualized using fluorescence microscopy using a Zeiss objective (ZEISS, Oberkochen, Germany) and a high-resolution colour camera (CIS Corporation, Japan). Images were reconstituted using ImageJ software. The area of TOMM20 staining, representing the mitochondrial network, was quantified using ImageJ software.

Apoptosis assessment

Basal or induced apoptosis was analysed using tert-butyl-hydroxide at 100 µM for half an hour using a luminescent assay measuring caspase 3 and 7 activities (Promega) in control and asthmatic BSM cells.

Western blot

Total cell and biopsy lysis was performed using a RIPA lysis buffer (Sigma-Aldrich). Total cellular extracts were loaded onto a 4-20% SDS-PAGE gel (Bio-Rad, Hercules, CA) and transferred onto a nitrocellulose membrane. Different commercial antibodies were used directed against Porin (Abcam), Citrate Synthase (Cell Signaling, Leiden, Netherlands), TOMM20 (Santa Cruz Biotechnologies, Dallas, TX), CPT1/CPT2 (Abcam and Life Invitrogen) and LDL-R (Abcam). HRP-coupled secondary antibodies were used for revelation using a ChemiDoc imaging instrument (Bio-Rad). Protein expression was normalized using total loading protein intensity (Stain-Free system Bio-Rad).

Label-free quantitative proteomics

Cells and tissue lysates were processed using RIPA buffer. Each lysate was centrifuged and the supernatant was used for the proteomic analysis at the Mass Spectrometry facility of Bordeaux University, as recently described [7]. Briefly, proteomic analysis was performed using an Ultimate 3000 RSLC Nano-UPHLC system (Thermo Fisher Scientific, Waltham, MA) coupled to a nanospray Orbitrap Fusion™ Lumos™ Tribrid™ Mass Spectrometer (Thermo Fisher Scientific, Waltham, MA).

These analyses were performed by the proteomics core facility at the University of Bordeaux (https://proteome.cgfb.u-bordeaux.fr/en). The steps of sample preparation and protein digestion were performed as previously described [8]. NanoLC-MS/MS analysis was performed using an Ultimate 3000 RSLC Nano-UPHLC system (Thermo Fisher Scientific) coupled to a nanospray Orbitrap Fusion™ Lumos™ Tribrid™ Mass Spectrometer (Thermo Fisher Scientific). Each peptide extract was loaded on a 300 µm ID x 5 mm PepMap C18 precolumn (Thermo Fisher Scientific) at a flow rate of 10 µL/min. After a 3 min desalting step, peptides were separated on a 50 cm EasySpray column (75 µm ID, 2 µm C18 beads, 100 Å pore size, ES803, Thermo Fischer Scientific) with a 4-40% linear gradient of solvent B (0.1% formic acid in 80% ACN) in 48 min. The separation flow rate was set at 300 nL/min. The mass spectrometer was operated in positive ion mode at a 2.0 kV needle voltage. Data were acquired using Xcalibur 4.1 software in a data-dependent mode. MS scans (m/z 375-1500) were recorded at a resolution of R = 120000 (@ m/z 200) and an AGC target of 4×105 ions collected within 50 ms, followed by a top speed duty cycle of up to 3 seconds for MS/MS acquisition. Precursor ions (2 to 7 charge states) were isolated in the quadrupole with a mass window of 1.6 Th and fragmented with HCD@30% normalized collision energy. MS/MS data were acquired in the ion trap with rapid scan mode,

AGC target of 3x103 ions and a maximum injection time of 300 ms. Selected precursors were excluded for 60 seconds. For protein identification, Sequest HT and Mascot 2.4 algorithms were used through Proteome Discoverer 1.4 Software (Thermo Fisher Scientific) for protein identification in batch mode by searching against a UniProt Homo sapiens database (71 536 entries, release March 2018). Two missed enzyme cleavages were allowed. Mass tolerances in MS and MS/MS were set to 10 ppm and 0.6 Da. Oxidation of methionine, deamidation of asparagine and glutamine, acetylation of lysine and N-terminal acetylation of the protein were searched as dynamic modifications. Carbamidomethylation on cysteine was searched as a static modification. Peptide validation was performed using the Percolator algorithm [9] and only "high confidence" peptides were retained corresponding to a 1% false discovery rate (FDR) at the peptide level. Raw LC-MS/MS data were imported into Progenesis QI (version 2.0 ; Nonlinear Dynamics, a Waters Company) for feature detection, alignment, and quantification. All sample features were aligned according to retention times by manually inserting up to fifty landmarks followed by automatic alignment to maximally overlay all the two-dimensional (m/z and retention time) feature maps. Singly charged ions and ions with charge states higher than six were excluded from the analysis. All remaining features were used to calculate a normalization factor for each sample to correct for experimental variation. Peptide identifications (with FDR < 1%) were imported into Progenesis. Univariate one-way analysis of variance (ANOVA) was performed within Progenesis LC–MS to calculate the protein p-value according to the sum of the normalized abundances across all runs. Only proteins with a p-value cut-off < 0.05 were validated. A minimum of two unique peptides matched to a protein, and a ≥ 1.2-fold change in relative abundance between the two conditions ($n = 5$ in each group) were used as the criteria for identification as a differentially expressed protein. Noticeably, only non-conflicting features and

unique peptides were considered for calculation at the protein level. The mass spectrometry proteomics data have been deposited to the ProteomeXchange Consortium via the PRIDE [10] partner repository with the dataset identifier PXD015566. Proteins were clustered according to their functions by using the Kyoto Encyclopedia of Genes and Genome Analysis in the search tool for retrieval of interactions between genes and proteins (STRING) database. A more global analysis of the data was performed using Ingenuity Pathway Analysis (IPA; Qiagen). We used the 'Core Analysis' package to identify relationships, mechanisms, functions, and pathways relevant to a dataset. We also used the 'regulators' package to identify predicted regulators of the proteomic changes. Comparative analyses were also performed with IPA using the 'Comparative Analysis' module.

Matrix-Assisted Laser Desorption/Ionization (MALDI) - mass spectrometry imaging analysis

Patient biopsies were frozen at -80°C and then embedded in a gel of 5% carboxymethyl cellulose. Serial cryosections (12 µm-thick) were cut from bronchial biopsies at -20°C using a NX70 Star cryostat (Thermo Fisher Scientific) and thaw-mounted onto standard glass microscope slides for MALDI - mass spectrometry imaging. These acquisitions were performed using a high performance atmospheric pressure imaging ion source named AP-SMALDI 5 AF (TransMIT GmbH) connected to an orbital trapping mass spectrometer (QExactive Orbitrap, Thermo Fisher Scientific). After MALDI - mass spectrometry imaging, we performed an α-smooth muscle actin immunostaining to localize the BSM area. We then estimated the relative lipid content within the BSM on the MALDI images. Fatty acid annotation was performed using the Human Metabolome Data Base and METASPACE software.

MALDI Acquisition

For the MALDI-MSI (matrix-assisted laser desorption/ionization) analysis of fatty acids, a homogenous matrix layer of 1,5-diaminonaphthalene (DAN, Sigma-Aldrich) was deposited using a home-built pneumatic sprayer [11]. Briefly, 150 µL of a 5 mg/ml of DAN matrix diluted in 70% acetone (30% mQ water) was applied to the tissues under the following optimized conditions: a 0.05 mL/min matrix solution flow rate and 0.9 bar of nitrogen gas flow rate. The matrix solution was supplemented with 1-palmitoyl-d31-2-oleoyl-sn-glycero-3-phosphate (16:0-d31-18:1 PA, Avanti Polar Lipid) at 0.2 mg/ml used as internal mass calibration during MS acquisition (the selected peak with the strongest signal was 16:0-d30-18:1 PA, [M - H]- m/z 703.6697 ± 0.003) and with palmitic acid-d31 (Sigma-Aldrich) at 0.2 mg/ml used as internal standards for fatty acid normalization ([M - H]- signal (m/z 286.4275 ± 0.003)). MALDI-MSI acquisitions were performed using a high performance atmospheric pressure imaging ion source named AP-SMALDI5 AF (TransMIT GmbH) connected to an orbital trapping mass spectrometer (QExactive Orbitrap, Thermo Fisher Scientific) [12]. This latter was operated in negative ion mode at a mass resolution of 70 000 at *m/z* 400 over a mass range of *m/z* 190-2000. The ion source was equipped with a diode laser (Flare NX343, λ = 343 nm), operating at a repetition rate of 2 kHz. Imaging data were acquired in high speed continuous mode with a pixel size of 18 µm and a speed rate of 3.7 pixels/s. Fatty acid annotation was performed using the Human Metabolome Data Base (HMBD) and METASPACE software [13] based on peak exact mass and isotope profiles. MALDI images were generated using MSiReader software [14].

Normalized ion images of fatty acids were generated by dividing the given fatty acid signal by the palmitic acid-d31 signal (m/z 286.4275 ± 0.003).

Co-registration of MALDI-MS images and histology

Following the acquisition of the MALDI images, the matrix was washed from the tissue surface by immersing the tissue for 10 seconds into a bath of 50% of acetone. Tissue sections were immersed in acetone before rapid permeabilization in PBS 1X- Triton 0.01% for 5 min. After rinsing in PBS 1X-Tween 0.1%, slides were incubated with blocking solution for 20 min with PBS 1X- 0.5% BSA. Tissue sections were incubated for 45 min at room temperature with α-Smooth Muscle Actin-FITC (Thermo Fisher Scientific). Tissue sections were then washed with PBS 1X--Tween 0.1% and incubated with nuclear staining DAPI for 5 min at room temperature. Tissue sections were mounted using an aqueous mounting medium (Sigma-Aldrich). Slides were scanned by using a digital slide scanner (Nanozzomer, Hamamatsu, Shizuoka, Japan) (Supplemental figure 1). Images were read by using NDP view software (Hamamatsu). Immunohistochemistry (IHC) and MALDI images were aligned as previously described [15, 16]. Briefly, for alignment, MALDI images of ion maps of m/z 885.549 (an endogenous phospholipid) and m/z 593.8317 (a matrix-related ion) were used to reveal the contours of the tissue border (Supplemental figure 9). The MALDI image was rescaled and aligned with the tissue bright field image using the contour and tissue defaults as guides. Then, the IHC image can be cropped at the size of the MALDI image to be loaded into MSiReader software. In this way, the confocal image is aligned with the whole MSI dataset allowing us to define ROIs based on the BSM area and epithelial area. To have the same robustness for all samples despite different BSM areas, we defined a measuring box with a size of 3x3 pixels (Supplemental figure

10) and performed in each tissue 18 measurements of fatty acid abundances in the different areas presenting BSM or epithelial cells in each tissue.

REFERENCES

1. Reddel HK, Hurd SS, FitzGerald JM. World Asthma Day. GINA 2014: a global asthma strategy for a global problem. *Int J Tuberc Lung Dis* 2014: 18(5): 505-506.
2. Crapo RO, Casaburi R, Coates AL, Enright PL, Hankinson JL, Irvin CG, MacIntyre NR, McKay RT, Wanger JS, Anderson SD, Cockcroft DW, Fish JE, Sterk PJ. Guidelines for methacholine and exercise challenge testing-1999. This official statement of the American Thoracic Society was adopted by the ATS Board of Directors, July 1999. *Am J Respir Crit Care Med* 2000: 161(1): 309-329.
3. Bara I, Ozier A, Girodet PO, Carvalho G, Cattiaux J, Begueret H, Thumerel M, Ousova O, Kolbeck R, Coyle AJ, Woods J, Tunon de Lara JM, Marthan R, Berger P. Role of YKL-40 in bronchial smooth muscle remodeling in asthma. *Am J Respir Crit Care Med* 2012: 185(7): 715-722.
4. Trian T, Benard G, Begueret H, Rossignol R, Girodet PO, Ghosh D, Ousova O, Vernejoux JM, Marthan R, Tunon-de-Lara JM, Berger P. Bronchial smooth muscle remodeling involves calcium-dependent enhanced mitochondrial biogenesis in asthma. *J Exp Med* 2007: 204(13): 3173-3181.
5. Trian T, Allard B, Dupin I, Carvalho G, Ousova O, Maurat E, Bataille J, Thumerel M, Begueret H, Girodet PO, Marthan R, Berger P. House dust mites induce proliferation of severe asthmatic smooth muscle cells via an epithelium-dependent pathway. *Am J Respir Crit Care Med* 2015: 191(5): 538-546.
6. Heuillet M, Bellvert F, Cahoreau E, Letisse F, Millard P, Portais JC. Methodology for the Validation of Isotopic Analyses by Mass Spectrometry in Stable-Isotope Labeling Experiments. *Anal Chem* 2018: 90(3): 1852-1860.
7. Henriet E, Abou Hammoud A, Dupuy JW, Dartigues B, Ezzoukry Z, Dugot-Senant N, Leste-Lasserre T, Pallares-Lupon N, Nikolski M, Le Bail B, Blanc JF, Balabaud C, Bioulac-Sage P, Raymond AA, Saltel F. Argininosuccinate synthase 1 (ASS1): A marker of unclassified hepatocellular adenoma and high bleeding risk. *Hepatology* 2017: 66(6): 2016-2028.

8. Esteves P, Dard L, Brillac A, Hubert C, Sarlak S, Rousseau B, Dumon E, Izotte J, Bonneu M, Lacombe D, Dupuy JW, Amoedo N, Rossignol R. Nuclear control of lung cancer cells migration, invasion and bioenergetics by eukaryotic translation initiation factor 3F. *Oncogene* 2019.
9. Kall L, Canterbury JD, Weston J, Noble WS, MacCoss MJ. Semi-supervised learning for peptide identification from shotgun proteomics datasets. *Nat Methods* 2007: 4(11): 923-925.
10. Perez-Riverol Y, Csordas A, Bai J, Bernal-Llinares M, Hewapathirana S, Kundu DJ, Inuganti A, Griss J, Mayer G, Eisenacher M, Perez E, Uszkoreit J, Pfeuffer J, Sachsenberg T, Yilmaz S, Tiwary S, Cox J, Audain E, Walzer M, Jarnuczak AF, Ternent T, Brazma A, Vizcaino JA. The PRIDE database and related tools and resources in 2019: improving support for quantification data. *Nucleic Acids Res* 2019: 47(D1): D442-D450.
11. Bouschen W, Schulz O, Eikel D, Spengler B. Matrix vapor deposition/recrystallization and dedicated spray preparation for high-resolution scanning microprobe matrix-assisted laser desorption/ionization imaging mass spectrometry (SMALDI-MS) of tissue and single cells. *Rapid Commun Mass Spectrom* 2010: 24(3): 355-364.
12. Kompauer M, Heiles S, Spengler B. Atmospheric pressure MALDI mass spectrometry imaging of tissues and cells at 1.4-mum lateral resolution. *Nat Methods* 2017: 14(1): 90-96.
13. Palmer A, Phapale P, Chernyavsky I, Lavigne R, Fay D, Tarasov A, Kovalev V, Fuchser J, Nikolenko S, Pineau C, Becker M, Alexandrov T. FDR-controlled metabolite annotation for high-resolution imaging mass spectrometry. *Nat Methods* 2017: 14(1): 57-60.
14. Robichaud G, Garrard KP, Barry JA, Muddiman DC. MSiReader: an open-source interface to view and analyze high resolving power MS imaging files on Matlab platform. *J Am Soc Mass Spectrom* 2013: 24(5): 718-721.
15. Blanc L, Daudelin IB, Podell BK, Chen PY, Zimmerman M, Martinot AJ, Savic RM, Prideaux B, Dartois V. High-resolution mapping of fluoroquinolones in TB rabbit lesions reveals specific distribution in immune cell types. *Elife* 2018: 7.
16. Blanc L, Lenaerts A, Dartois V, Prideaux B. Visualization of Mycobacterial Biomarkers and Tuberculosis Drugs in Infected Tissue by MALDI-MS Imaging. *Anal Chem* 2018: 90(10): 6275-6282.

SUPPLEMENTAL DATAS AND FIGURE LEGENDS

Supplemental table 1: Representation of protein expression among "mitochondrial dysfunction" annotation box

Protein	Uniprot accession number	Log2 (Fold Change)	-Log10 (p value)
CPT2	**P23786**	**1.615**	**1.789**
NDUFB11	Q9NX14	1.187	1.571
CASP8	E7EQ06	1.161	1.748
SLC27A3	H7BZH4	1.118	0.232
TXNRD2	Q9NNW7	0.891	1.054
MT-ND1	P03886	0.846	1.819
NDUFS8	E9PKH6	0.758	1.865
NDUFA10	A0A087WXC5	0.733	2.798
ACAA1	P09110	0.684	1.972
FIS1	Q9Y3D6	0.621	2.638
SDHC	Q99643	0.516	0.143
CYB5A	P00167	0.509	1.228
NDUFAF2	Q8N183	0.472	1.590
NDUFB9	Q9Y6M9	0.467	1.370
GPX4	A0A0A0MTT1	0.462	0.635
MAP2K4	P45985	0.430	0.745
NDUFA7	O95182	0.404	0.592
ACSL1	P33121	0.391	0.895
NDUFS6	O75380	0.382	0.528

GPX7	Q96SL4	0.377	0.671
NDUFA9	Q16795	0.353	0.960
NDUFS5	O43920	0.333	0.849
IVD	P26440	0.318	1.131
NDUFV1	G3V0I5	0.307	0.767
ECHS1	P30084	0.300	1.144
NDUFA6	P56556	0.283	1.057
NDUFA5	Q16718	0.280	0.441
NDUFB10	O96000	0.273	2.184
NDUFS2	O75306	0.253	0.908
ECI1	P42126	0.253	0.489
HSD17B10	Q99714	0.250	1.405
HSD17B10	Q99714	0.250	1.405
ACAA2	P42765	0.250	0.893
NDUFS1	P28331	0.242	0.738
GSR	P00390	0.236	0.513
NDUFA8	P51970	0.235	1.687
NDUFA12	Q9UI09	0.234	0.380
APP	H7C0V9	0.231	0.273
ACO2	A2A274	0.220	0.917
HADH	Q16836	0.213	0.557
OGDH	Q02218	0.207	0.726
PRDX5	P30044	0.195	0.509

NDUFA11	Q86Y39	0.179	0.056
ATP5PD	O75947	0.172	0.639
NDUFS3	O75489	0.167	0.909
NDUFA13	Q9P0J0	0.161	0.458
MT-ND2	P03891	0.154	0.356
NDUFV2	P19404	0.153	0.479
CYB5R3	P00387	0.143	0.920
NDUFB6	O95139	0.138	1.078
PARK7	Q99497	0.135	0.832
PRDX3	P30048	0.124	0.635
NDUFB7	P17568	0.107	0.315
UQCRC1	P31930	0.087	0.371
CYC1	P08574	0.085	0.363
CPT1A	P50416	0.084	0.332
NDUFB4	O95168	0.083	0.117
UQCRFS1	P47985	0.081	0.242
CYCS	P99999	0.079	0.566
ECI2	A0A0C4DGA2	0.077	0.086
RHOT2	Q8IXI1	0.073	0.152
ATP5F1A	P25705	0.070	0.340
ATP5F1B	P06576	0.065	0.393
COX5B	P10606	0.061	0.063
ATP5PO	P48047	0.057	0.295

ATP5F1C	P36542	0.055	0.361
UQCRC2	P22695	0.055	0.220
NDUFB5	E7EWP0	0.045	0.198
MAOA	P21397	0.036	0.088
MAPK10	A0A286YF97	0.036	0.048
ATP5PB	Q5QNZ2	0.034	0.217
COX6B1	P14854	0.029	0.076
PDHA1	P08559	0.019	0.079
HSD17B4	P51659	0.007	0.001
HADHA	P40939	0.003	0.019
ACO1	P21399	0.001	0.012
NCSTN	Q92542	0.000	0.018
MT-CO2	P00403	-0.006	0.016
SDHB	P21912	-0.013	0.024
ATP5F1D	P30049	-0.014	0.043
HADHB	P55084	-0.014	0.009
COX4I1	P13073	-0.029	0.145
HTRA2	A0A0C4DG44	-0.045	0.078
ATP5MF	P56134	-0.058	0.285
MT-ATP6	P00846	-0.059	0.153
GPD2	P43304	-0.076	0.203
NDUFB3	O43676	-0.076	0.141
MAPK8	A6NF29	-0.092	0.243

MT-CO3	P00414	-0.094	0.027
SOD2	P04179	-0.110	0.100
ACSL3	O95573	-0.118	0.605
COX7C	P15954	-0.145	0.419
SCP2	P22307	-0.153	0.525
SDHA	P31040	-0.158	0.369
AIFM1	O95831	-0.166	0.394
ACADM	B7Z9I1	-0.179	0.581
CAT	P04040	-0.200	0.483
UQCRB	P14927	-0.213	0.600
CASP3	P42574	-0.225	1.435
VDAC3	Q9Y277	-0.240	0.524
VDAC1	P21796	-0.256	0.662
UQCRQ	O14949	-0.271	1.444
VDAC2	A0A0A0MR02	-0.315	0.713
ATP5MG	E9PN17	-0.335	1.412
COX5A	H3BRM5	-0.347	1.788
NDUFA4	O00483	-0.371	0.907
SLC27A4	Q6P1M0	-0.390	1.505
COX7A2L	E5RJZ1	-0.487	0.277
COX6C	P09669	-0.490	1.361
ATP5ME	P56385	-0.520	3.013
ACSL4	O60488	-0.882	0.427

Supplemental figure S1: Identification of BSM cells and epithelium in patient bronchial biopsies

(A) Representative images of non-asthmatic and asthmatic biopsies obtained after MALDI-MSI and immunostaining experiments, showing linoleate MSI data (red), alpha smooth muscle actin staining (green) and DAPI (blue) of whole non-asthmatic and asthmatic biopsies with the corresponding crop area. **(B)** Representative immunofluorescence images of non-asthmatic and asthmatic biopsies showing BSM with α-smooth muscle actin (α-SMA, green) staining. **(C)** Bright field images and DAPI staining of bronchial epithelium in non-asthmatic and asthmatic biopsies. Nuclei are stained with DAPI (blue).

Supplemental figure S2: Blocking fatty acid oxidation has no effect on bronchial epithelial cell proliferation

BrdU incorporation was assessed in bronchial epithelial cells (n=4) in the absence (-) or in the presence (+) of 10 nM etomoxir **(A)** or 10 nM perhexilin **(B)** for 24 hours. Data are presented as dot plots with the median. NS indicates not significant using Wilcoxon statistical test.

Supplemental figure S3: Transduction efficiency in asthmatic BSM cells

Asthmatic BSM cells were transduced with either a scrambled shRNA (-) or an anti-CPT2 shRNA (+). **(A)** Transduction efficiency was measured using GFP positive staining and flow cytometry (n=3). Quantification of immunoblots for CPT2 **(B**, n=4**)** or CPT1 **(C**, n=3**)** protein expression levels. Stain free gel technology was used for loading control expression quantification. Data are presented as dot plots with the median. * $P<0.05$ using the Wilcoxon statistical test. NS indicates not significant.

Supplemental figure S4: CPT2 shRNA transduction in non-asthmatic BSM cells

Cell proliferation was assessed in non-asthmatic BSM cells (n=3) transduced with either a scrambled shRNA lentivirus (-) or an anti-CPT2 shRNA lentivirus (+), by Ki67 positive staining using flow cytometry **(A)** and cell counting **(B)**. Data are presented as dot plots with the median. * $P<0.05$ using the Wilcoxon statistical test.

Supplemental figure S5: Blocking fatty acid entry and oxidation has no effect on BSM cell apoptosis

Basal apoptosis was analysed by measuring caspases 3 and 7 activities by bioluminescence assay in non-asthmatic (white circles, n=4) and asthmatic (black squares, n=4) BSM cells following treatment with 10 nM etomoxir **(A)**, 10 nM perhexilin **(B)**, or 5 µg/mL anti-LDL-R blocking antibody **(C)**, for 5 days. Data are presented as dot plots with the median. NS indicates not significant using the Wilcoxon statistical test.

Supplemental figure S6: Blocking fatty acid oxidation and entry has no effect on mitochondrial mass remodelling in asthmatic BSM cells

Immunoblot analysis of mitochondrial mass markers, including porin **(A and D)**, citrate synthase **(B and E)** and TOMM20 **(C and F)** protein expression levels in asthmatic BSM cells in the absence (-) or in the presence (+) of 10 nM etomoxir (n=4), 10 nM perhexilin (n=4), 5 µg/mL anti-LDL-R (n=4) or CPT2 shRNA (n=3) treatment for 5 days. Stain-free gel technology was used for loading control expression quantification. Data are presented as dot plots with the median. NS indicates not significant using one-way ANOVA and Wilcoxon statistical tests.

Supplemental figure S7: Steroid and LABA effects on CPT2 and LDL-R expression in asthmatic BSM cells

Representative image and quantification of CPT2 **(A)** and LDL-R **(B)** immunoblot protein expression in asthmatic BSM cells (n=4) cultured in the presence (+) or in the absence (-) of 10^{-7}M salmeterol (Sal), 10^{-8}M fluticasone (Flu), 10^{-7}M formoterol (For), or 10^{-8}M budesonide (Bud), alone or in combination. Stain free gel technology was used for loading control expression quantification. Data are presented as dot plots with the median. NS indicates not significant using one-way ANOVA statistical test.

Supplemental figure S8: Steroid and LABA effects on ATP content in asthmatic BSM cells

Steady-state ATP content was measured in asthmatic (n=4) BSM cells cultured in the presence (+) or in the absence (-) of fluticasone **(A)**, salmeterol with fluticasone **(B)**, budesonide **(C)** and formoterol with budesonide **(D)**. Data are presented as dot plots with the median. NS indicates not significant using one-way ANOVA and Wilcoxon statistical tests.

Supplemental figure S9: MALDI-MSI alignment with brigh tfield and IHC images

(A) Brigh tfield image. **(B)** MALDI-MSI of endogenous phospholipids (PI 38:4, m/z 885,549 in green). **(C)** MALDI-MSI of exogenous matrix-related compounds (m/z 593.8317 in blue).

(D) Overlay of exogenous and endogenous compound MALDI-MSI used as guides for the imprint and contour of tissue, respectively. **(E)** Overlay of endogenous compound MALDI-MSI and bright field image. **(F)** Overlay of bright field images with exogenous and endogenous compound MALDI-MSI.

Supplemental figure S10: Relative quantification of fatty acid abundance by MALDI-MSI

(A) Tissue IHC image. **(B)** Magnification of the region in the orange rectangle in **(A)**. **(C)** Overlay of IHC image with fatty acid (linoleate) MALDI-MSI (in greyscale). **(D)** Fatty acid (linoleate) MALDI-MSI (in greyscale) with a 3×3 pixel measuring box (pink square). In all IHC images, DAPI is shown in blue and smooth muscle actin is shown in red.

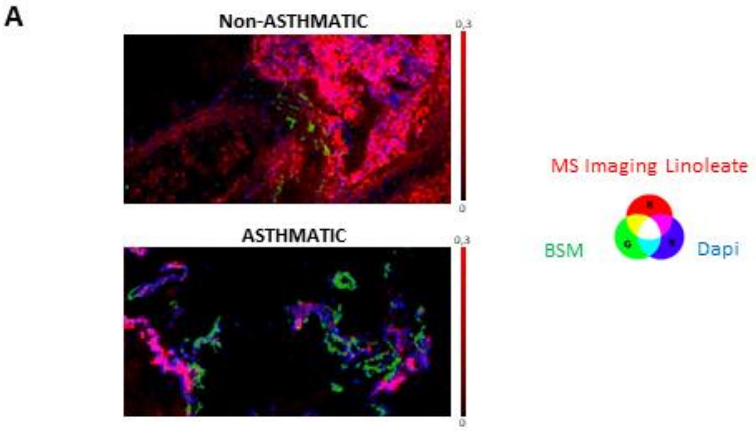

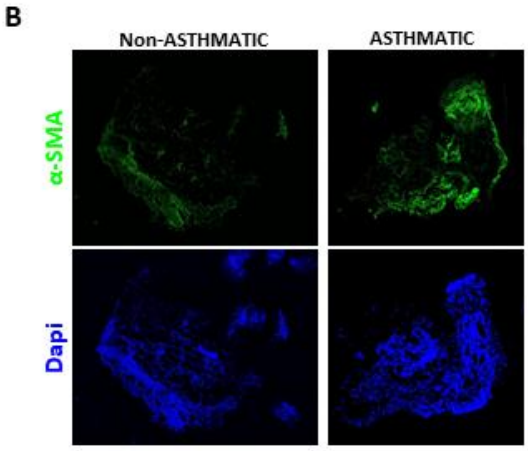

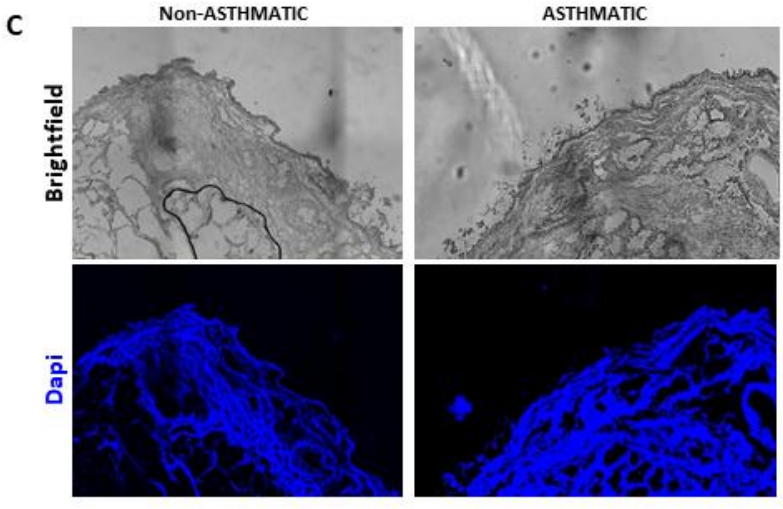

Supplemental figure S1

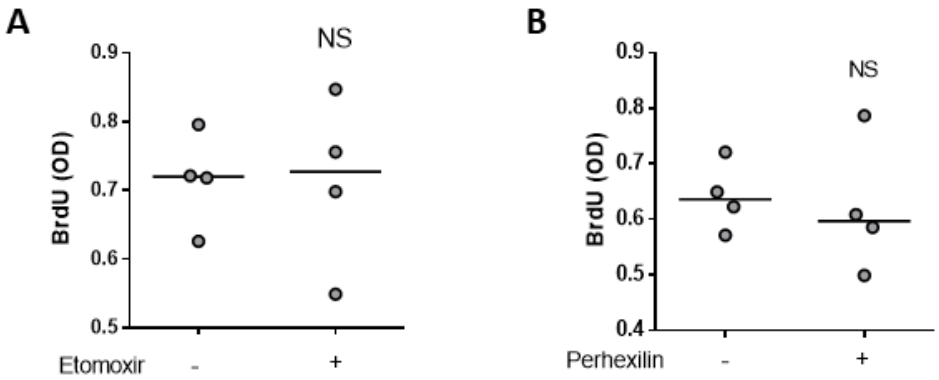

Supplemental figure S2

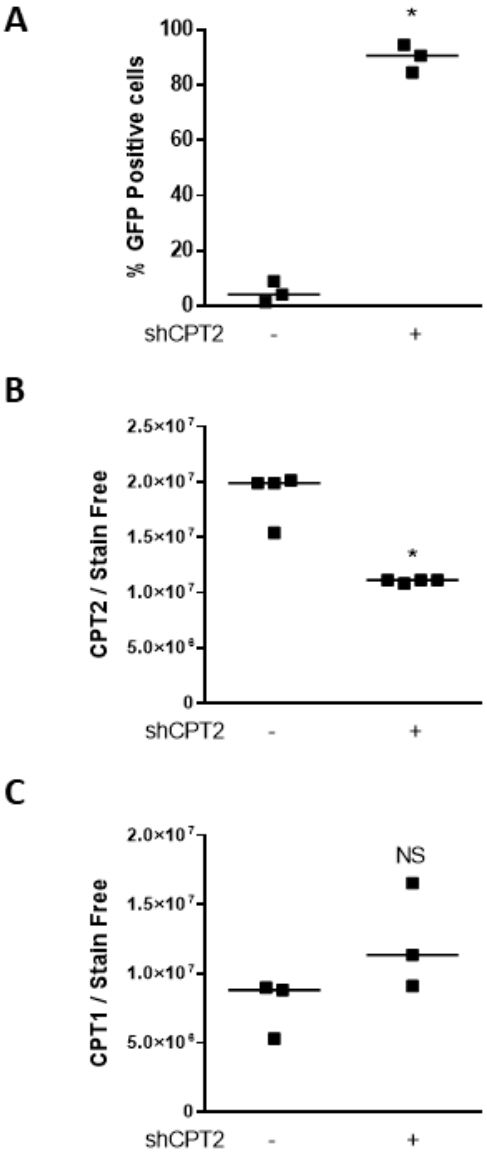

Supplemental figure S3

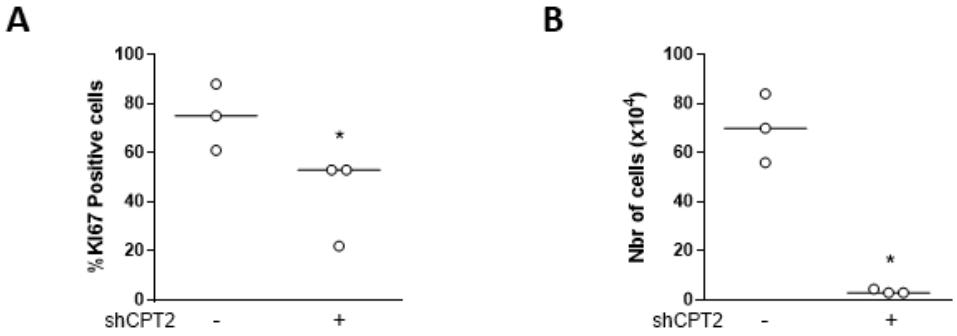

Supplemental figure S4

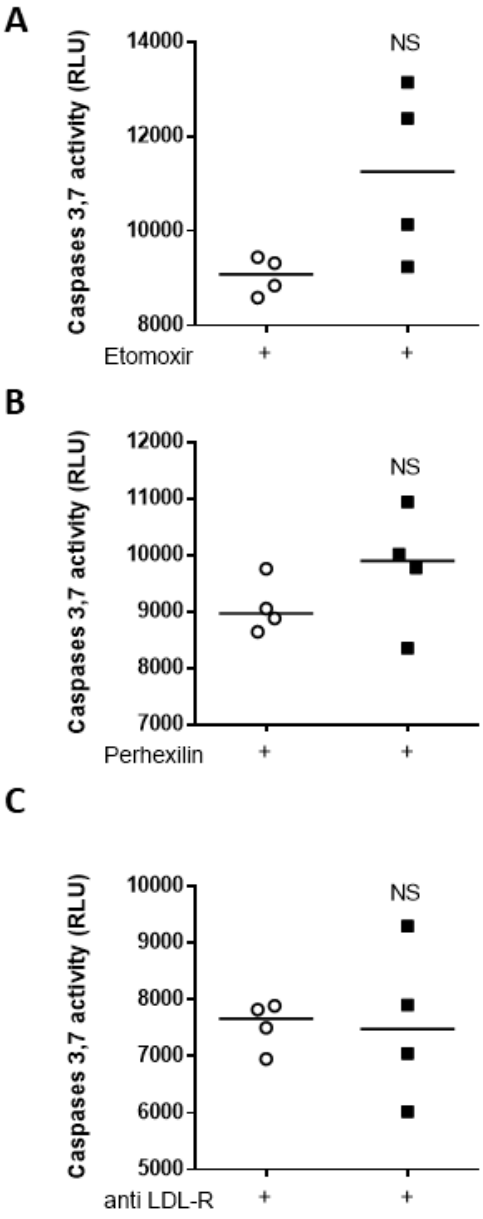

Supplemental figure S5

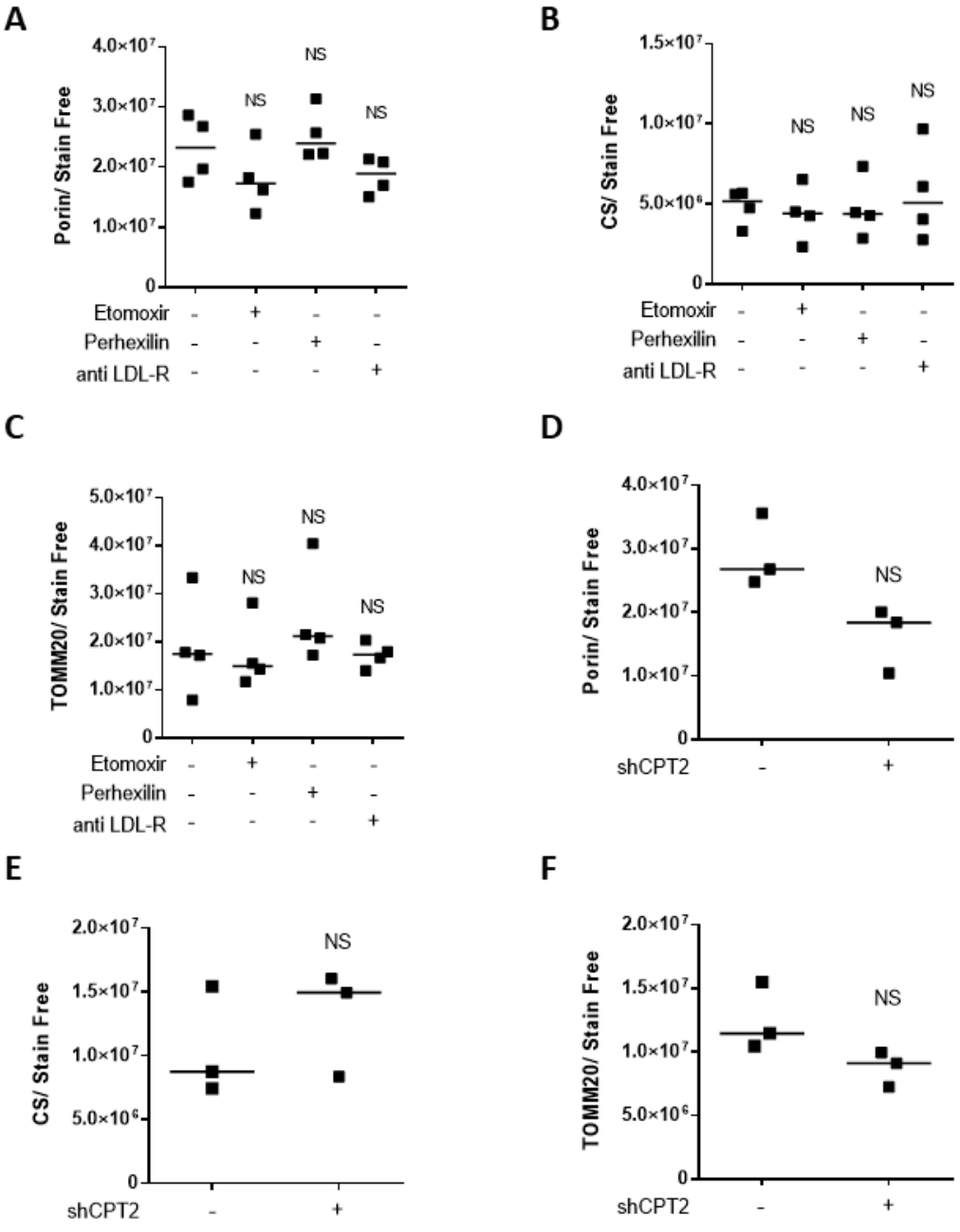

Supplemental figure S6

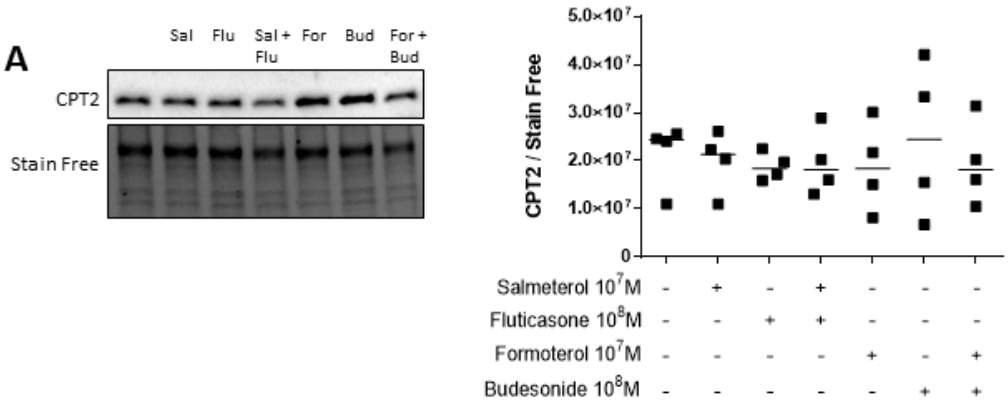

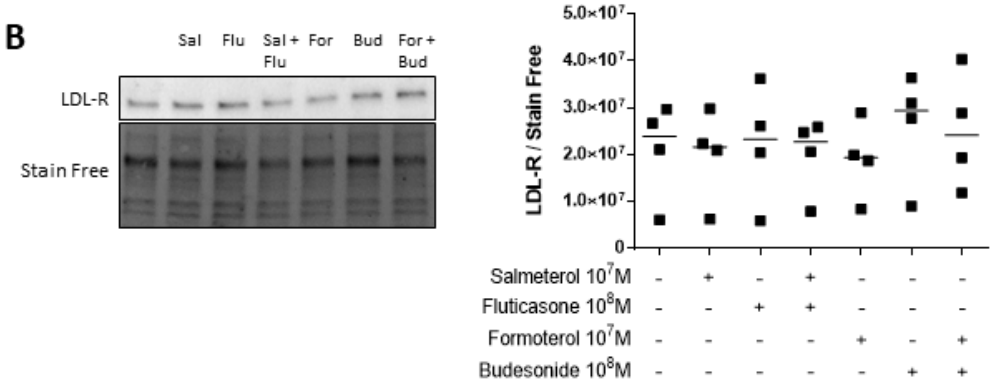

Supplemental figure S7

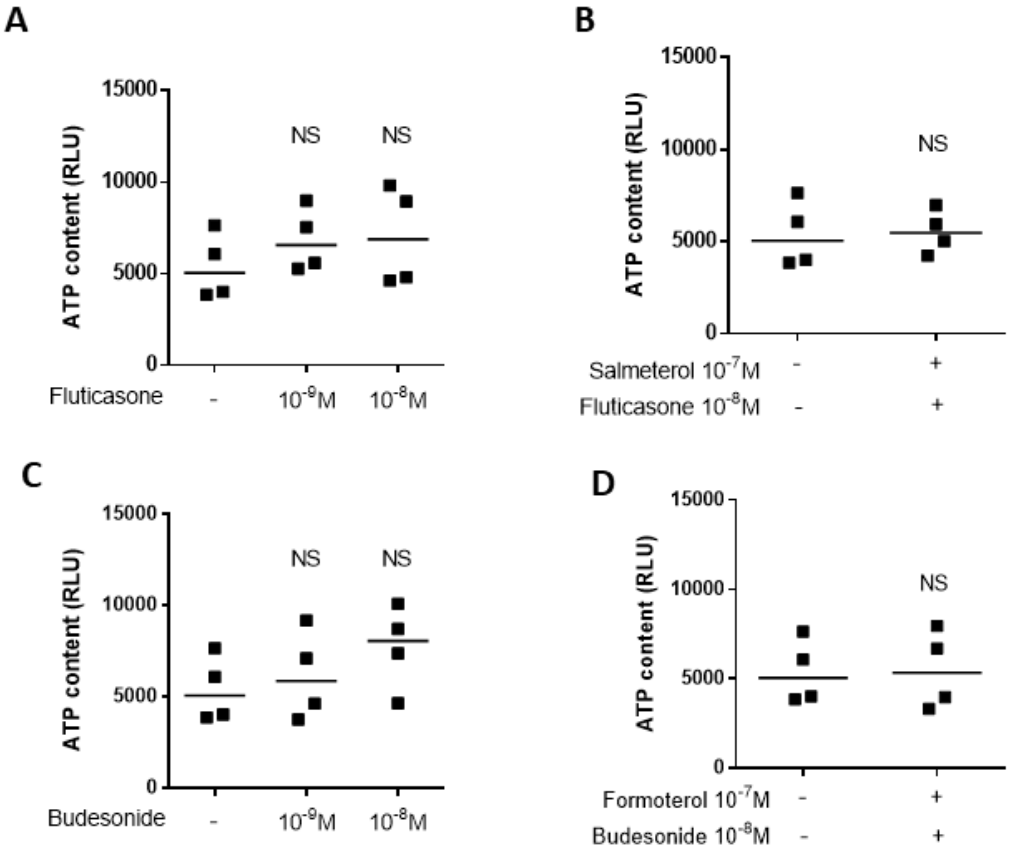

Supplemental figure S8

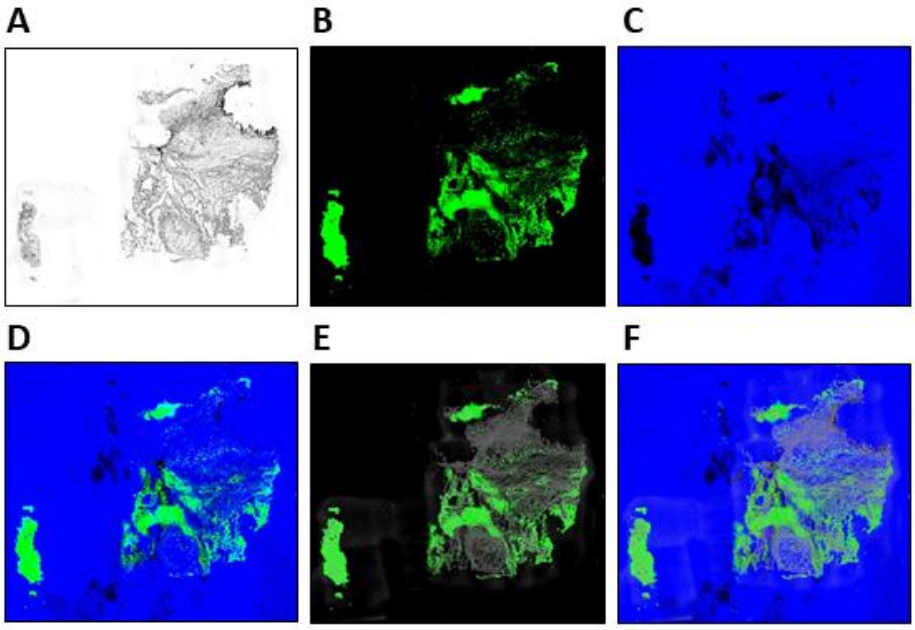

Supplemental figure S9

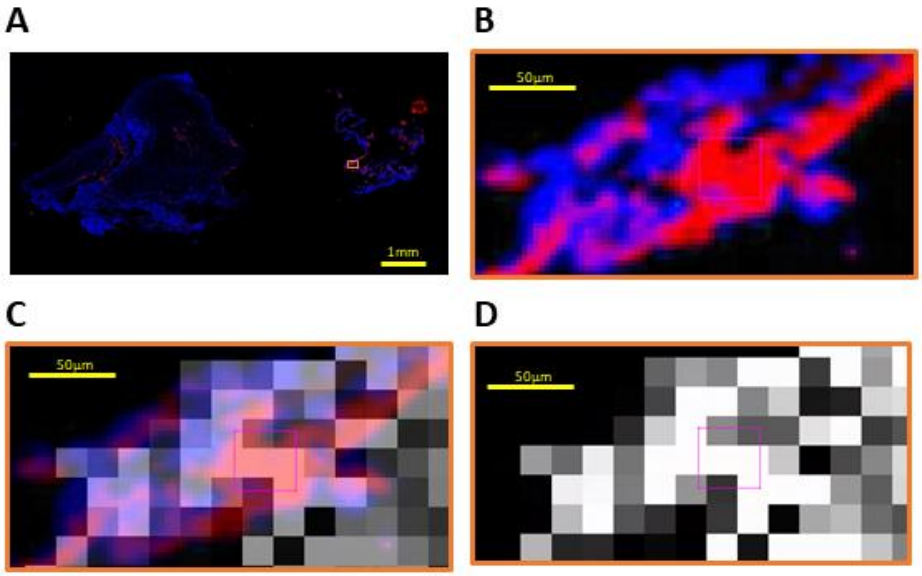

Supplemental figure S10